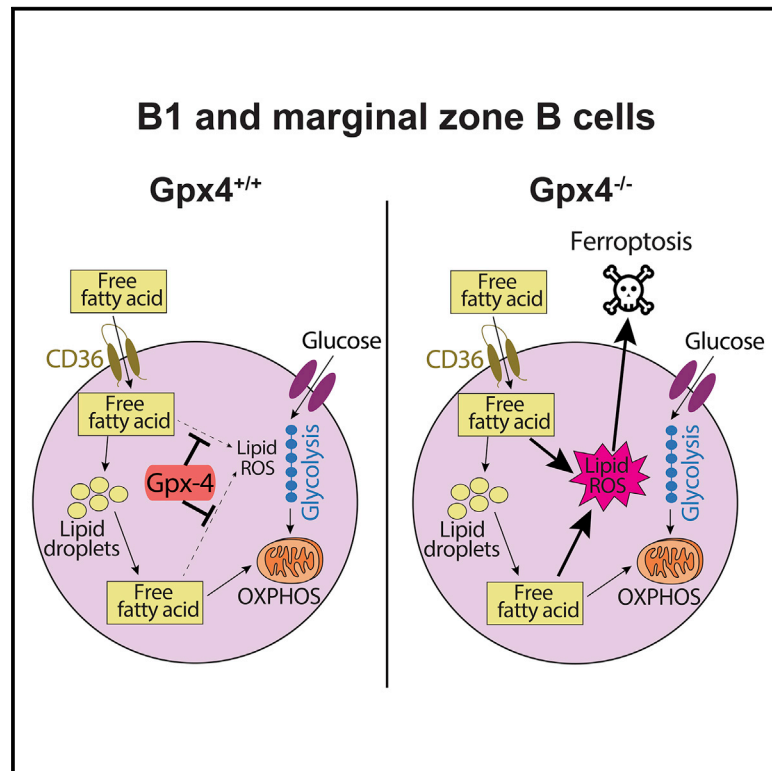


B1 and Marginal Zone B Cells but Not Follicular B2 Cells Require Gpx4 to Prevent Lipid Peroxidation and Ferroptosis

Graphical Abstract



Authors

Jonathan Muri, Helen Thut,
Georg W. Bornkamm, Manfred Kopf

Correspondence

manfred.kopf@ethz.ch

In Brief

Muri et al. demonstrate that B1 and marginal zone (MZ) B cells but not follicular (Fo) B2 cells require Gpx4 during homeostasis and antibody responses. Mechanistically, B1 and MZ B cells display increased lipid metabolism, sensitivity to lipid peroxidation, and ferroptosis in comparison to Fo B cells.

Highlights

- Gpx4 is required for the maintenance and antibody responses of B1 and MZ B cells
- Gpx4^{-/-} Fo B cells can develop and undergo normal germinal-center reactions
- Gpx4 prevents lipid peroxidation and ferroptosis in B1 and MZ B cells
- Gpx4 allows increased lipid metabolism in B1 and MZ B compared to Fo B2 cells



B1 and Marginal Zone B Cells but Not Follicular B2 Cells Require Gpx4 to Prevent Lipid Peroxidation and Ferroptosis

Jonathan Muri,¹ Helen Thut,¹ Georg W. Bornkamm,² and Manfred Kopf^{1,3,*}

¹Institute of Molecular Health Sciences, ETH Zurich, 8093 Zürich, Switzerland

²Institute of Clinical Molecular Biology and Tumor Genetics, Helmholtz Zentrum München, 85764 Neuherberg, Germany

³Lead Contact

*Correspondence: manfred.kopf@ethz.ch

<https://doi.org/10.1016/j.celrep.2019.10.070>

SUMMARY

Aerobic organisms need to maintain cellular redox homeostasis. Glutathione peroxidase-4 (Gpx4) has the unique ability to protect cells against lipid peroxidation. Here, we show that Gpx4 is absolutely required to prevent ferroptosis during development, maintenance, and responses of innate-like B cells, namely, the B1 and marginal zone (MZ) B cells. In contrast, Gpx4 is dispensable for the development, germinal center reactions, and antibody responses of follicular B2 cells. Mechanistically, we show increased lipid metabolism and sensitivity to lipid peroxidation and ferroptosis in B1 and MZ B cells compared to follicular B2 cells, consistent with the requirement of Gpx4 in innate-like B cells. This high sensitivity to ferroptosis of innate-like B cells may be used to therapeutically target Gpx4 in certain forms of B cell malignancies involving B1 cells.

INTRODUCTION

Regulation of the cellular redox state is crucial for cell function and survival. Reactive oxygen species (ROS) are chemically reactive molecules containing oxygen, which are generated by aerobic organisms as a result of normal cellular metabolism. The main sources of endogenously produced ROS include NADPH oxidases and electron transport in the mitochondrial respiratory chain (D'AuRéaux and Toledano, 2007). At low concentrations, ROS are critically required for physiological cellular processes, where they regulate cell proliferation, differentiation, and death. By contrast, high concentrations of ROS can damage cellular macromolecules such as lipids, nucleic acids, and proteins, thereby leading to cell death and contributing to the physiology of aging (Birben et al., 2012; Finkel, 2011; Finkel and Holbrook, 2000; Ray et al., 2012). The imbalance between ROS and antioxidants in favor of ROS, termed as oxidative stress, has been described to contribute to various diseases, such as cancer (Toyokuni et al., 1995), asthma (Andreadis et al., 2003; Comhair et al., 2005), diabetes (Brownlee, 2001), and neurological disorders (Jenner, 2003; Lyras et al., 1997).

Aerobic organisms have evolved a sophisticated cellular anti-oxidant defense network to keep ROS at homeostatic levels in the cell. Part of this system is made up by glutathione peroxidases (Gpx), an enzyme family composed of 8 enzymes with the biological role to protect the organism from oxidative damage. They utilize glutathione (GSH) as a source of electrons to reduce hydrogen peroxide or organic peroxides to water or the corresponding alcohols, respectively (Brigelius-Flohé and Maiorino, 2013). Interestingly, only a sole member of the Gpx family, Gpx4, possesses the ability to directly reduce phospholipid hydroperoxides and oxidized lipoproteins, thereby protecting cells against membrane lipid peroxidation (Roveri et al., 1994; Thomas et al., 1990). A systemic deletion of Gpx4 is embryonically lethal, which highlights the critical role of this protein isoform for development and cellular function (Yant et al., 2003).

Recently, it has been established that Gpx4 is critical to prevent cells from ferroptosis, an iron-dependent oxidative form of cell death associated with increased lipid ROS and impaired capacity to scavenge lipid peroxides (Dixon et al., 2012). Ferroptosis can be triggered by physiological conditions (e.g., increased extracellular concentrations of glutamate), by small molecules that block the Cys₂/glutamate antiporter system x_c⁻, or by the genetic ablation of Gpx4 (Dixon, 2017; Dixon et al., 2012; Friedmann Angeli et al., 2014; Maiorino et al., 2018; Matsushita et al., 2015). Indeed, Gpx4 has a central role in preventing ferroptosis by converting toxic lipid-associated hydroperoxides to harmless organic alcohols. It has been now increasingly recognized that, in some cases, metabolic reprogramming of cancer cells is associated with higher sensitivity to ferroptosis, therefore establishing novel anti-cancer strategies (Friedmann Angeli et al., 2019; Seibt et al., 2019).

Whereas the absence of Gpx4 has been demonstrated to cause renal failure (Friedmann Angeli et al., 2014), hepatocyte degeneration (Carlson et al., 2016), and neuroinflammation (Hambright et al., 2017), the understanding of Gpx4 in distinct cell types has not been rigorously studied. We have previously described the importance of Gpx4 for prevention of lipid peroxidation and ferroptosis upon T cell activation, thus allowing efficient immunity to infection (Matsushita et al., 2015). However, the role of Gpx4 in other immune cells has not been addressed so far. Here, we report that unlike T cells follicular (Fo) B2 cells do not require Gpx4 for development, homeostatic maintenance, germinal center (GC) reactions, and antibody responses.



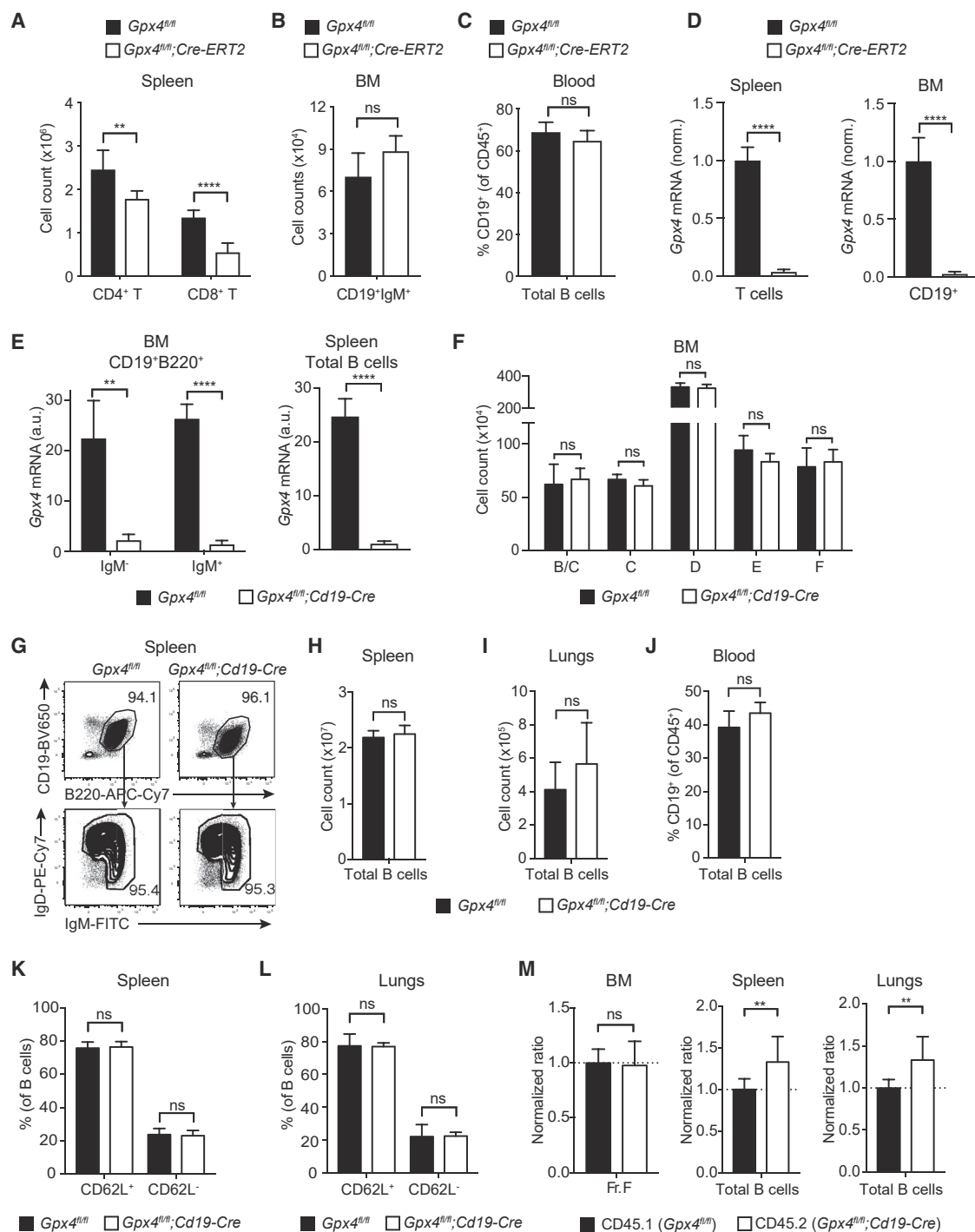


Figure 1. *Gpx4* Is Dispensable for B Cell but Not T Cell Development and Homeostasis

(A–D) *Gpx4*^{fl/fl};Cre-ERT2 mice and control *Gpx4*^{fl/fl} littermates were injected with TAM to delete the *Gpx4* gene and analyzed by flow cytometry 1 week later. (A–C) Total numbers of splenic CD4⁺ and CD8⁺ T cells (A) and of CD19⁺IgM⁺ B cells in the bone marrow (BM; B) and percentage of CD19⁺ B cells in the blood (C); n = 4–5. (D) Analysis of *Gpx4* mRNA in MACS-enriched CD90⁺ T cells in the spleen (left) and CD19⁺ B cells in the BM (right) by real-time PCR (n = 4). (E–L) Analysis of the different B cell populations in naive *Gpx4*^{fl/fl};Cd19-Cre and *Gpx4*^{fl/fl} littermate control mice. (E) Analysis of *Gpx4* mRNA in FACS-sorted IgM⁻ and IgM⁺ CD19⁺B220⁺ populations in the BM (left) and in splenic CD19⁺B220⁺ B cells (right) by real-time PCR (n = 3–4). (F) The quantifications of the indicated Hardy B cell fractions are shown (n = 6).

(legend continued on next page)

By contrast, we found that Gpx4 is essential in B1 and marginal zone (MZ) B cells during development, maintenance, and for antibody responses to *Streptococcus pneumoniae*. Indeed, B1 and MZ B cells lacking Gpx4 accumulate lipid peroxidation and die by ferroptosis due to their high uptake of fatty acids to sustain metabolic functions. These results consequently suggest that therapeutically targeting Gpx4 might be beneficial in forms of leukemia where B1 cells are known to be involved.

RESULTS

Gpx4 Is Dispensable for the Development and Maintenance of Fo B2 Cells

We have previously described the crucial role of Gpx4 in protecting activated T cells from accumulation of lipid peroxides and cell death by ferroptosis (Matsushita et al., 2015). In this context, we now aim to investigate the importance of Gpx4 in the other main type of lymphocytes, the B cells. To address this, we generated *Gpx4^{fl/fl};Cre-ERT2* mice by crossing mice with loxP-flanked *Gpx4* alleles to mice carrying tamoxifen (TAM)-inducible *Cre-ERT2*. As expected from our previous study (Matsushita et al., 2015), TAM administration to *Gpx4^{fl/fl};Cre-ERT2* mice led to a significant reduction in total CD4⁺ and CD8⁺ T cells in the spleen (Figure 1A). To our surprise, however, total CD19⁺IgM⁺ B cell numbers in the bone marrow and the percentage of CD19⁺ B cells in the blood were comparable in TAM-treated *Gpx4^{fl/fl};Cre-ERT2* and control (*Gpx4^{fl/fl}*) mice (Figures 1B and 1C). We additionally verified that Cre-mediated deletion in both T and B cells of *Gpx4^{fl/fl};Cre-ERT2* mice was complete at the mRNA level upon TAM administration (Figure 1D). Together, these results suggest a distinct requirement of the Gpx4 antioxidant pathway in T and B lymphocytes.

To further study this interesting difference in the requirement of Gpx4 between B and T lymphocytes, we generated *Gpx4^{fl/fl};Cd19-Cre* mice. The deletion of *Gpx4* was expectedly complete at the mRNA level in both IgM[−] and IgM⁺ CD19⁺B220⁺ B cells in the bone marrow and in total CD19⁺ B cells in the spleen of *Gpx4^{fl/fl};Cd19-Cre* mice (Figure 1E). We next studied B cell development via flow cytometry using the Hardy classification system, which subdivides distinct B cell developmental stages into fraction A (pre/pro-B cells), fraction B (pro-B cells), fraction C (large pre-B cells), fraction D (small pre-B cells), fraction E (immature B cells), and fraction F (mature B cells) (Hardy et al., 1991). All of these fractions were intact in *Gpx4^{fl/fl};Cd19-Cre* compared *Gpx4^{fl/fl}* littermate control mice (Figure 1F). Furthermore, numbers of mature IgM⁺IgD⁺CD19⁺B220⁺ B cells in the spleen (Figures 1G

and 1H), inguinal lymph nodes (iLNs; Figure S1A), lungs (Figure 1I), and their percentage in the blood (Figure 1J) were not affected by *Gpx4* deficiency. We additionally verified that the activation status of B cells as determined by measurement of CD62L surface expression also remained unaffected in these organs in the absence of *Gpx4* (Figures 1K and 1L; Figure S1B). To further confirm our findings, we investigated the ability of *Gpx4*-deficient B cells to refill the hematopoietic compartment of lethally irradiated hosts in a competitive situation with wild-type (WT) cells. Lethally irradiated WT C57BL/6 mice (CD45.1⁺CD45.2⁺) were reconstituted with an equal ratio of congenically marked donor bone marrow cells from *Gpx4^{fl/fl};Cd19-Cre* mice (CD45.2⁺) and WT (CD45.1⁺) mice. *Gpx4*-deficient B cells were able to contribute similarly to Fraction F in the bone marrow as well as to the peripheral B cell compartments in the spleen, lungs, iLNs, and in the blood (Figure 1M; Figure S1C), as WT B cells. Overall, these data demonstrate that, in contrast to an important role for T cell homeostasis (Matsushita et al., 2015), *Gpx4* is dispensable for the development and maintenance of Fo B2 cells.

Gpx4 Is Dispensable for B Cell Antibody Responses and GC Reactions

With the help of follicular helper CD4⁺ T cells (Tfh), Fo B cells undergo GC reactions to give rise to high-affinity antibody responses. Since we have shown that *Gpx4* is completely dispensable for the development and homeostatic maintenance of Fo B cells, we next sought to understand whether *Gpx4* plays a role in the production of antibodies during an *in vivo* response. Thus, we immunized *Gpx4^{fl/fl};Cd19-Cre* and *Gpx4^{fl/fl}* control mice with replication-defective Q β -virus-like particles (Q β -VLPs) containing *E. coli* single-stranded RNA (ssRNA) and monitored Q β -VLP-specific antibody levels on days 7, 18, and 32 post-infection. *Gpx4^{fl/fl};Cd19-Cre* and *Gpx4^{fl/fl}* mice mounted comparable Q β -VLP-specific immunoglobulin M (IgM) (Figure 2A) and class-switched IgG2b (Figure 2B) antibody responses. Q β -VLPs not only trigger vigorous antibodies responses but also induce GC reactions, such as hypermutations, affinity maturation, and B cell memory (Bachmann et al., 1995; Bachmann and Zinkernagel, 1997; Jennings and Bachmann, 2008). Therefore, we also analyzed B cells in the GC by flow cytometry on day 7 post-infection with Q β -VLPs. GC B cells are generally defined by the marker profile B220⁺CD38^{low}Fas⁺ and can be further subdivided into CXCR4⁺ dark zone (DZ) and CD86⁺ light zone (LZ) cells (Vic-tora et al., 2010). Interestingly, *Gpx4^{fl/fl};Cd19-Cre* mice showed a higher frequency in GC B cells compared to the *Gpx4^{fl/fl}* controls (Figures 2C and 2D), and no difference in distribution between

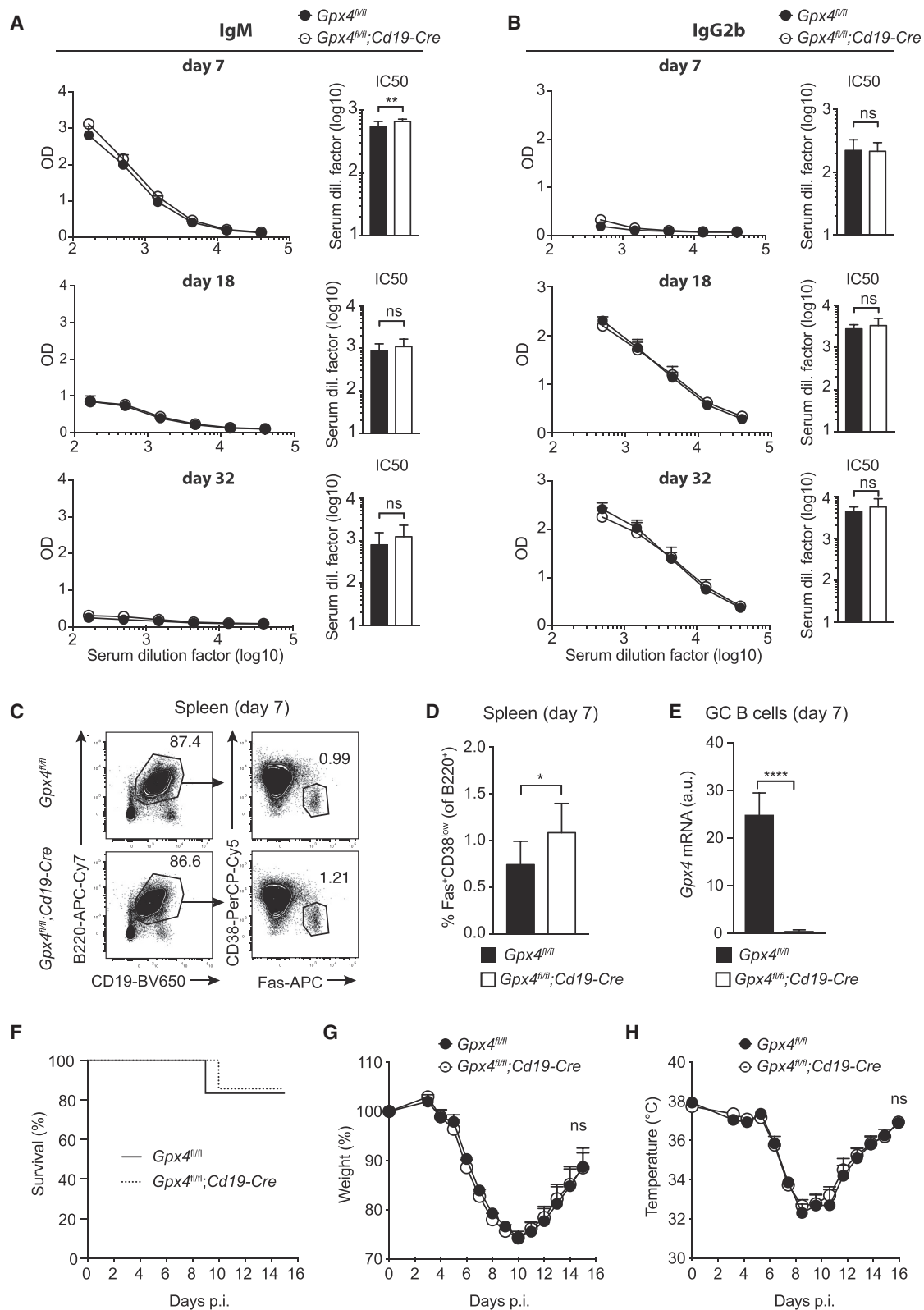
(G and H) Representative FACS plots (G) and quantification (H) of total mature B cells in the spleen (n = 6).

(I and J) The total B cell counts in the lungs (I) and percentage of B cells in the blood (J) are depicted. (n = 6).

(K and L) Expression of CD62L on CD19⁺ B cells from the spleen (K) and lungs (L); n = 6).

(M) Lethally irradiated WT mice were reconstituted with a 1:1 mixture of WT and *Gpx4^{fl/fl};Cd19-Cre* BM cells expressing the congenic markers CD45.1 and CD45.2, respectively. After reconstitution, the contribution of *Gpx4^{fl/fl};Cd19-Cre* to the indicated populations in the BM (left), spleen (middle), and lungs (right) was assessed. Values were normalized to non-Cre expressing congenic marker-matched TCR β ⁺ T cells, followed by normalization such that CD45.1⁺ WT cell contribution to the respective population equals 1. Values <1 or >1 indicate reduced or higher contribution of *Gpx4^{fl/fl};Cd19-Cre* cells to the B cell population relative to WT cells, respectively (n = 10). Bar graphs show mean \pm SD. Numbers "n" represent individual mice. Numbers in the FACS plots indicate the percentage of the depicted gates. Data are representative of two (A–E and M) and three (F–L) independent experiments. Student's t test (two-tailed, unpaired) was used for the comparison of two groups (A–F and H–M): *p \leq 0.05; **p \leq 0.01; ***p \leq 0.001; ****p \leq 0.0001; ns, not significant.

See also Figures S1 and S5.



(legend on next page)

LZ and DZ cells was observed between both groups (Figures S2A and S2B). Since the *Cd19-Cre* system is notoriously leaky and a few escapees might seed the GC in *Gpx4^{fl/fl};Cd19-Cre* mice, we fluorescence-activated cell sorted (FACS) B220⁺CD38^{low}Fas⁺ GC B cells from both *Gpx4^{fl/fl};Cd19-Cre* and *Gpx4^{fl/fl}* groups and verified that *Gpx4* deletion was complete at the mRNA level (Figure 2E).

We further confirmed the dispensability of *Gpx4* in B cells in a more potent mouse model of infectious disease by infecting *Gpx4^{fl/fl};Cd19-Cre* and *Gpx4^{fl/fl}* control mice with the replicating influenza A virus PR8. Survival, temperature and weight loss in the course of disease were comparable in both groups of mice (Figures 2F–2H), which was additionally reflected in the comparable PR8-specific antibody response kinetics (Figures S2C and S2D). Taken together, *Gpx4* is dispensable for development, homeostasis, and antibody responses of Fo B cells.

B1 and MZ B Cells Require *Gpx4* for Development and Homeostasis

B cells can be divided into several subclasses that differ in ontogeny, homeostasis, and functionality. B1 cells can be subdivided into B1a and B1b cells, while B2 cells encompass Fo and MZ B cells. While the predominant Fo B cells are important for immune responses against thymus-dependent antigens, B1 and MZ B cells rapidly respond to blood-borne antigens with antibody production independent of T cell help (Baumgarth, 2011; Pillai and Cariappa, 2009). We found that the numbers and frequencies of splenic CD23⁺ Fo B cells were comparable in *Gpx4^{fl/fl};Cd19-Cre* and *Gpx4^{fl/fl}* mice, whereas CD21⁺CD23[−] MZ B cells were significantly reduced in the absence of *Gpx4* (Figures 3A and 3B). We next investigated whether the different developing splenic B cell subsets (Allman and Pillai, 2008), which give rise to the mature MZ B cells, also exhibited a similar reduction in numbers due to *Gpx4* deficiency (Figures S3A and S3B). However, we observed similar numbers of transitional T1 and T2 cells, Fo type I and type II cells, and MZ precursors (MZPs) in *Gpx4*-sufficient and -deficient mice, thus suggesting that the steady-state maintenance of MZ B cells rather than their maturation in the spleen is impaired in the absence of *Gpx4* (Figure 3C; Figure S3C). Furthermore, *Gpx4* deletion also led to reduced frequency and numbers of total CD19⁺CD43⁺CD23[−] B1 cells in the spleen (Figures 3D and 3E). The predominant B1 subset CD5⁺ B1a was strikingly affected, although a significant reduction was also observed in the minor

CD5[−] B1b subset (Figures 3D, 3F, and 3G). Since B1 cells are highly enriched in the peritoneal cavity, we next investigated the effect of *Gpx4* deficiency in this compartment. We found significantly reduced numbers and frequencies of total CD19⁺B220⁺ B cells in the peritoneal cavity of *Gpx4^{fl/fl};Cd19-Cre* compared to WT control mice (Figures 3H and 3I). In line with the results in the spleen, the frequency of B1 cells was also reduced in the peritoneal cavity, and, as a consequence, we observed a higher percentage of B2 cells in the absence of *Gpx4* (Figures 3J and 3K). Importantly, *Gpx4* deletion led to drastically reduced numbers of B1a and B1b cells, while the B2-cell compartment remained unaffected (Figures 3L and 3M). To further analyze the various stages of peritoneal B1 cells, we next utilized the CD11b marker, which was shown to be expressed by nearly half of the cells in each of the peritoneal B1 populations (B1a and B1b) (Ghosh et al., 2008). We found that both CD11b⁺ and CD11b[−] B1a and B1b cell subsets are significantly reduced in numbers in the absence of *Gpx4* (Figures 3J and 3N). Together, while *Gpx4* is dispensable for Fo B cells, these data indicate that it is required for the development and homeostasis of B1 and MZ B cells.

To further study this differential requirement of *Gpx4* by distinct B cell subsets in a competitive situation, WT C57BL/6 mice (CD45.1⁺CD45.2[−]) were lethally irradiated and reconstituted with an equal ratio of congenically marked donor bone marrow cells from *Gpx4^{fl/fl};Cd19-Cre* mice (CD45.2⁺) and WT (CD45.1⁺) mice. While the Fo B cell pool was similarly reconstituted by both *Gpx4*-deficient and WT cells, MZ B cells were reconstituted mainly by WT cells (Figure 3O), consistent with the reduced MZ B cell numbers we observed in naive *Gpx4^{fl/fl};Cd19-Cre* mice compared to *Gpx4^{fl/fl}* controls (Figure 3B). Furthermore, B1 cells (both B1a and B1b) were also outcompeted to a higher proportion by WT cells compared to B2 cells (Figures 3P and 3Q), also in line with the results observed in non-chimeric mice (Figures 3K–3M). Here, it is important to note that, despite being fetal in origin, the B1-cell pool can be reconstituted by bone-marrow precursors upon steady-state perturbations, such as B1-cell depletion due to irradiation (Düeber et al., 2009; Holodick et al., 2009). However, this process is less efficient, as it can be observed by the fact that B1 cells, which generally are the predominant B cell population in the peritoneal cavity at the steady-state, represent only 10% of total peritoneal B cells after bone-marrow reconstitution of lethally irradiated mice (Figure S3D). Overall, these data demonstrate

Figure 2. *Gpx4* Is Not Required for B Cell-Mediated Antibody Responses and GC Reactions

(A–E) *Gpx4^{fl/fl};Cd19-Cre* mice and *Gpx4^{fl/fl}* littermate control mice were immunized with Q β -VLPs containing *E. coli* ssRNA. (A and B) Mice were bled at day 7 (top), 18 (middle), and 32 (bottom) after immunization to determine Q β -VLP-specific IgM (A) and IgG2b (B) antibody responses via ELISA (n = 6). Each panel depicts plots of OD_{405nm} against serum dilutions (left) and IC₅₀ (right) for Q β -VLP-specific antibodies. (C and D) GC B cells in the spleen as defined by the expression profile Fas⁺CD38^{low} were analyzed by flow cytometry on day 7 post-immunization (n = 5–7). Gating strategy of Fas⁺CD38^{low} B cells in the spleen (pre-gated on live/CD45⁺/TCR β [−]/F4/80[−]/Ly-6G[−]) (C). Percentage of Fas⁺CD38^{low} B cells in the spleen (D). (E) Analysis of *Gpx4* mRNA in FACS-sorted B220⁺CD38^{low}Fas⁺ GC B cells by real-time PCR (n = 4). (F–H) *Gpx4^{fl/fl};Cd19-Cre* mice and *Gpx4^{fl/fl}* littermate control mice were infected with 100 plaque-forming unit (PFU) PR8 influenza A virus (n = 4). Graph represents the survival curve (F). Weight (G) and temperature (H) were monitored as depicted in the graphs. Dot plots represent mean \pm SEM (A, B, G, and H). Bar graphs show mean \pm SD (A, B, D, and E). Numbers “n” represent individual mice. Numbers in the FACS plots indicate the percentage of the depicted gates (C). Data are representative of two (A, B, and E–H) and three (C and D) independent experiments. Student’s t test (two-tailed, unpaired) was used to compare *Gpx4^{fl/fl};Cd19-Cre* and *Gpx4^{fl/fl}* groups (A, B, D, and E): *p \leq 0.05; **p \leq 0.01; ****p \leq 0.0001; ns, not significant. Two-way ANOVA adjusted by Bonferroni’s multiple comparison test was used in (G) and (H): *p \leq 0.0332; ns, not significant. See also Figures S2 and S5.

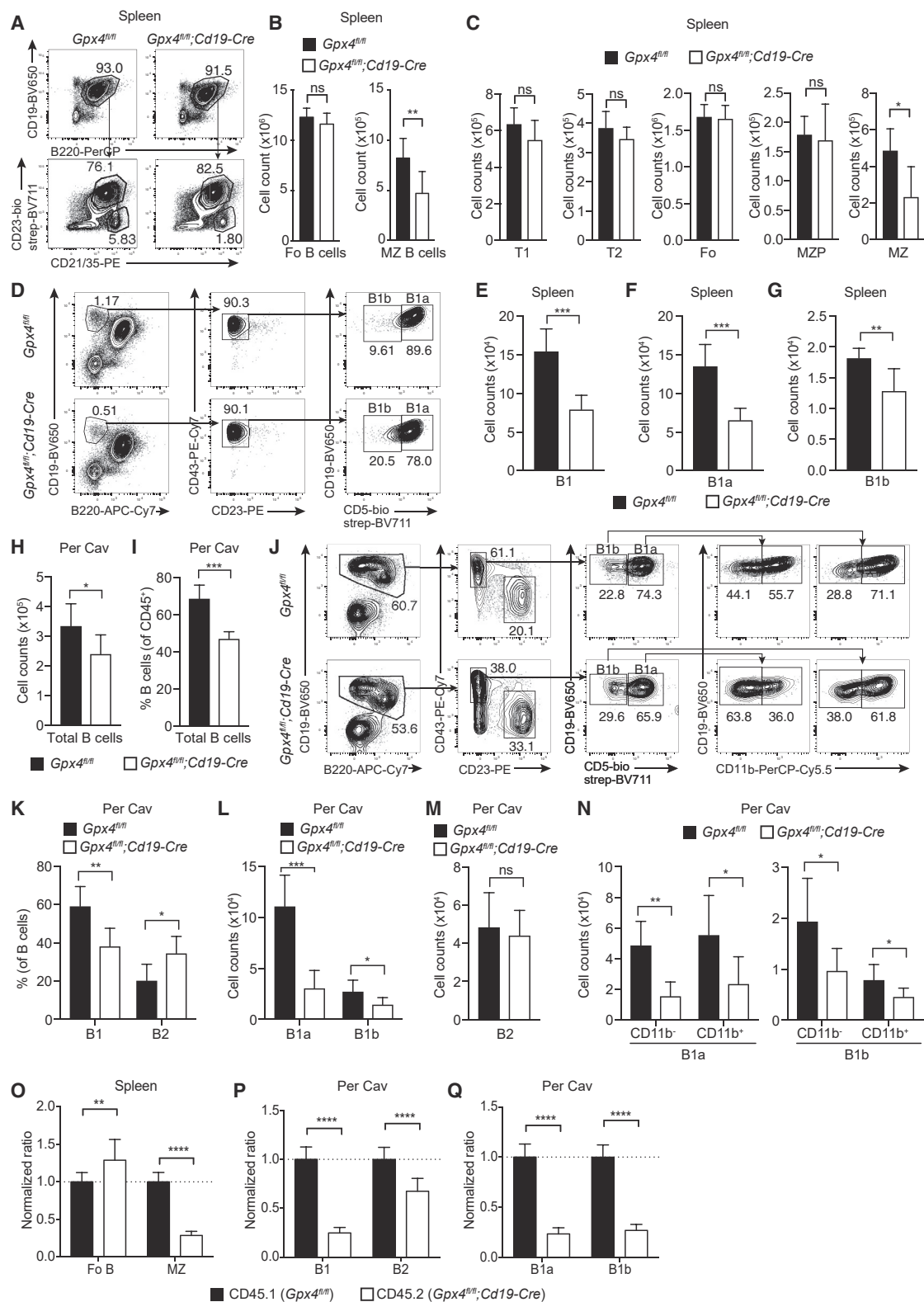


Figure 3. *Gpx4* Is Critical for the Homeostasis of B1 and MZ B Cells but Not Fo B2 Cells

(A–N) Analysis of the indicated B cell populations in naive *Gpx4*^{fl/fl};Cd19-Cre and *Gpx4*^{fl/fl} littermate control mice via flow cytometry. (A) Gating strategy of Fo (CD23⁺) and MZ (CD21/35⁺CD23⁺) B cells in the spleen (pre-gated on live/CD45⁺/CD11b⁺/TCRβ⁻).

(legend continued on next page)

the pivotal role of the Gpx4 antioxidant pathway in B1 and MZ B cells and imply distinct requirements of Gpx4 in the B2 and B1/MZ B cell populations.

Gpx4 Is Required to Mount an Efficient Antibody Response to *Streptococcus pneumoniae*

B1 and MZ B cells are indispensable for mounting low-affinity phosphorylcholine (PC)-specific IgM antibody responses to *Streptococcus pneumoniae* reaching the blood (Baumgarth, 2011; Martin et al., 2001; Tanigaki et al., 2002). Since we observed reduced numbers of both B1 and MZ B cells in the absence of Gpx4, we next aimed at studying the consequences of the reduction of these B cell populations in the context of antibody responses to *Streptococcus pneumoniae*. Therefore, we intravenously immunized mice with heat-inactivated bacteria and assessed the PC-specific IgM antibody response 5 days after immunization (Figure 4A). On day 0, PC-specific IgM antibody levels were low in the blood (Figure 4B). Five days after immunization, the Gpx4^{fl/fl} control group mounted a strong anti-PC IgM response, while the Gpx4^{fl/fl};Cd19-Cre mice had strikingly lower PC-specific IgM titers (Figures 4C and 4D). Together, these findings show that the defective development and homeostasis of B1 and MZ B cells in the absence of Gpx4 translates into an impaired antibody response to *Streptococcus pneumoniae*.

Gpx4 Prevents Lipid Peroxidation in B1 and MZ B Cells

Gpx4 has been described as a unique antioxidant enzyme for its ability to directly protect cells against membrane lipid peroxidation (Sattler et al., 1994; Thomas et al., 1990). Thus, we next wondered whether the B cell subsets, which were reduced in numbers in the absence of Gpx4, accumulated cellular lipid peroxides to a higher degree compared to unaffected subsets. To test this, we took advantage of the C11-BODIPY_{581/591} probe to stain for lipid ROS. Interestingly, we observed that a higher proportion of Gpx4-deficient B1 cells accumulated lipid peroxides in comparison to B2 cells in the peritoneal cavity (Figures 5A and 5B). Similarly, splenic B1 cells also accumulated lipid ROS to a greater extent compared to splenic B2 cells in the absence of Gpx4 (Figures 5C and 5D). Finally, we also detected

an increased percentage of MZ B cells with lipid peroxidation in Gpx4^{fl/fl};Cd19-Cre compared to Gpx4^{fl/fl} control mice (Figures 5C and 5D). Together, these results suggest that B1 and MZ B cells are reduced in the absence of Gpx4 due to toxic effects caused by the accumulation of lipid peroxides.

It has been recently described that B1a cells engage a metabolic program distinct from Fo B2 cells, which is characterized by increased glycolysis and fatty acid synthesis, as well as by the uptake of lipids and their storage in lipid droplets (Clarke et al., 2018). We thus hypothesized that these metabolic differences among the distinct B cell subsets might reflect their differential requirement of Gpx4. To expand on this possibility, we intravenously injected WT mice with the fluorescently labeled long-chain fatty acid palmitate (BODIPY FL C₁₆) and sacrificed them for analysis 1 h later. We observed that B1 cells have a strikingly increased fatty acid uptake compared to B2 cells in the peritoneal cavity (Figure 5E), in line with the recent report mentioned above (Clarke et al., 2018). In contrast to B1 and Fo B cells, little is known about the metabolic phenotype of MZ B cells. Therefore, we next compared fatty acid uptake between B1, Fo, and MZ B cells in the spleen. Interestingly, we found that splenic B1 cells take up the highest levels of fatty acids, while MZ B cells displayed an intermediate uptake rate still significantly higher than the one of Fo B cells (Figure 5F). Due to this similarity in the uptake of fatty acids between B1 and MZ B cells, we further analyzed expression of genes from the metabolic gene transcription signature of B1a cells (Clarke et al., 2018) using the ImmGen database. Consistent with the high rate in lipid uptake, both B1 and MZ B cells express higher levels of the fatty acid transporter protein CD36 in comparison to Fo B2 cells (Figure 5G). Moreover, they both have increased expression of *Plin3* [Perilipin-3] (Figure 5H), which has been described to participate in lipid droplet formation in B1a cells (Clarke et al., 2018). We next found that, similarly to B1 cells, MZ B cells also display increased levels of *Myc* [c-Myc], *Hk2* [Hexokinase 2], *Ldha* [Lactate dehydrogenase A], and *Gapdh* [Glyceraldehyde 3-phosphate dehydrogenase] (Figure 5I; Figure S4A–S4C) compared to Fo B2 cells, indicating increased levels of glycolysis at the steady state. Overall, these data suggest that both B1 and MZ B cells have similar metabolic features

(B) Shown are the total cell counts of Fo (left) and MZ (right) B cells in the spleen (n = 6).

(C) Shown are the total cell counts of developing splenic B cell subsets, including T1/T2 transitional cells, follicular type II (Fo-II) cells, and MZ precursors (MZPs). The reduction in mature MZ B cells is also depicted (n = 6).

(D) Gating strategy of splenic B1 cells, which can be further subdivided into B1a (CD5⁺) and B1b (CD5⁺) cells (pre-gated on live/CD45⁺/TCRβ⁺).

(E–G) Cell numbers of total B1 (E), B1a (F), and B1b (G) cells in the spleen are shown (n = 6).

(H and I) The absolute cell numbers (H) and frequencies (I) of total B cells (CD19⁺B220⁺) in the peritoneal cavity (Per Cav) was assessed (n = 6).

(J) Gating strategy of B1 (CD43⁺CD23⁺) and B2 (CD43⁺CD23⁺) cells in the peritoneal cavity (pre-gated on live/CD45⁺/F4/80⁺). B1 cells are further subdivided into B1a (CD5⁺) and B1b (CD5⁺) cells, and each of these B1 subsets is subsequently tested for the expression of the CD11b marker.

(K–N) Depicted are the percentages of B1 and B2 cells (K) and the cell numbers of B1a and B1b cells (L), of total B2 cells (M), and of the CD11b⁺ and CD11b⁺ populations among the B1a and B1b cell subsets (N) in the peritoneal cavity (n = 6).

(O–Q) Lethally irradiated WT mice were reconstituted with a 1:1 mixture of WT and Gpx4^{fl/fl};Cd19-Cre BM cells expressing the congenic markers CD45.1 and CD45.2, respectively. Upon reconstitution, contribution of WT and Gpx4^{fl/fl};Cd19-Cre cells to the indicated B cell populations in the spleen (O) and peritoneal cavity (P and Q) was assessed. Values were normalized to non-Cre expressing congenic marker-matched TCRβ⁺ T cells, followed by normalization such that CD45.1⁺ WT cell contribution to the respective population equals 1. Values <1 or >1 indicate reduced or higher contribution of Gpx4^{fl/fl};Cd19-Cre cells to the B cell population relative to WT cells, respectively (n = 10).

Bar graphs show mean ± SD. Numbers “n” represent individual mice. Numbers in the FACS plots indicate the percentage of the depicted gate. Data are representative of two (A–G and N–Q) and three (H–M) independent experiments. Student’s t test (two-tailed, unpaired) was used to compare two groups for statistical differences (B, C, E–I, and K–Q): *p ≤ 0.05; **p ≤ 0.01; ***p ≤ 0.001; ****p ≤ 0.0001; ns, not significant.

See also Figures S3 and S6.

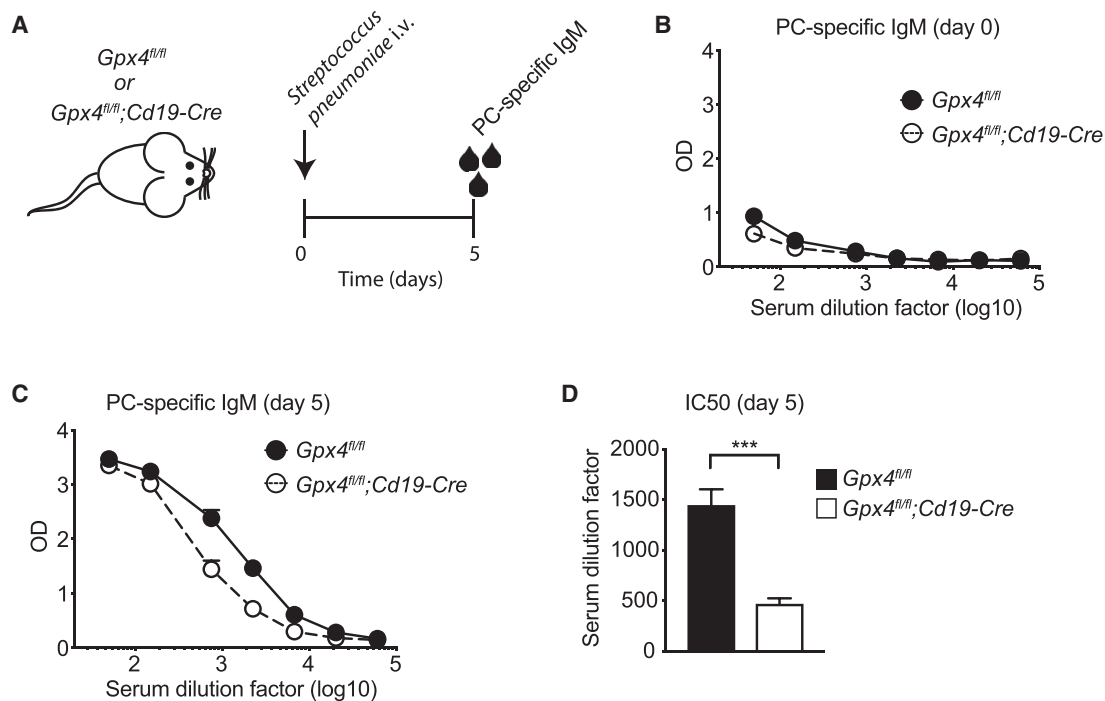


Figure 4. Gpx4 Is Required for IgM Antibody Responses to *Streptococcus pneumoniae*

Gpx4^{fl/fl};Cd19-Cre and Gpx4^{fl/fl} littermate control mice were infected with heat-inactivated *Streptococcus pneumoniae*, and mice were bled to determine phosphorylcholine (PC)-specific IgM titers by ELISA at day 0 and 5 after immunization (n = 4–5).

(A) Diagram showing the experimental design of the infection.

(B and C) Optical density (OD) values at day 0 (B) and 5 (C) upon *Streptococcus pneumoniae* immunization. Each panel depicts plots of OD_{405nm} (OD) against serum dilutions for PC-specific IgM antibodies.

(D) IC₅₀ for PC-specific IgM response 5 days after immunization. Dot plots and bar graphs represent mean ± SEM (B–D). Numbers “n” represent individual mice. Data are representative of two independent experiments. Student’s t test (two-tailed, unpaired) was used to compare Gpx4^{fl/fl};Cd19-Cre and Gpx4^{fl/fl} groups (D): ***p ≤ 0.001.

and that Gpx4 allows high lipid uptake by preventing lipid peroxidation.

B1 and MZ B Cells Die by Ferroptosis in the Absence of Gpx4

Accumulation of lipid peroxidation is well known to trigger ferroptosis, an iron-dependent, oxidative form of non-apoptotic cell death (Dixon, 2017; Dixon et al., 2012). We have previously described the role of Gpx4 in protecting activated T cells from the accumulation of lipid ROS and consequential ferroptosis (Matsushita et al., 2015). Thus, we next aimed to compare the survival of T and B cells lacking Gpx4. As expected from our previous study (Matsushita et al., 2015), Gpx4-deficient CD8⁺ and CD4⁺ T cells underwent massive cell death in the first 3 h after incubation independently of T cell receptor (TCR) stimulation (Figures 6A and 6B; data not shown). Notably, addition of the ferroptosis inhibitor ferrostatin-1 (Fer-1) completely abolished the cell death of Gpx4-deficient T cells, confirming cell death by ferroptosis (Figures 6A and 6B). In this study, we showed that Fo B2 cells did not require Gpx4 for development, homeostatic maintenance, and responses (Figures 1 and 2). In line with this, we observed that unlike T cells, splenic B cells survived normally in the absence of Gpx4 regardless of whether they were stimulated or not (Figures 6C and 6D). Together, these results confirm

the different requirement of the Gpx4 pathway in T and B lymphocytes.

We next wondered whether B1 and MZ B cells die by ferroptosis *ex vivo*. To test this, we FACS-sorted Fo B2 and MZ B cells from the spleen, and B1 and B2 cells from the peritoneal cavity, stimulated them with LPS and anti-IgM, and monitored cell survival. In contrast to splenic Fo B2 cells, we found that MZ B cells lacking Gpx4 die by ferroptosis *ex vivo*, since the cell death was completely prevented in the presence of Fer-1 (Figure 6E). Moreover, Gpx4-deficient B1 cells from the peritoneal cavity also underwent ferroptosis to a much greater extent in comparison to peritoneal B2 cells (Figure 6F), indicating that protection from ferroptosis by Gpx4 in metabolically active B1 cells is not a consequence of the particular environment (i.e., peritoneum). Overall, these data demonstrate that the accumulation of lipid ROS in Gpx4-deficient B1 and MZ B cells leads to cell death by ferroptosis.

DISCUSSION

A breakthrough in the immunometabolism field was achieved through studies in T cells showing that the activation of naive T cells, which mainly rely on oxidative phosphorylation (OXPHOS) for their metabolic requirements, leads to metabolic

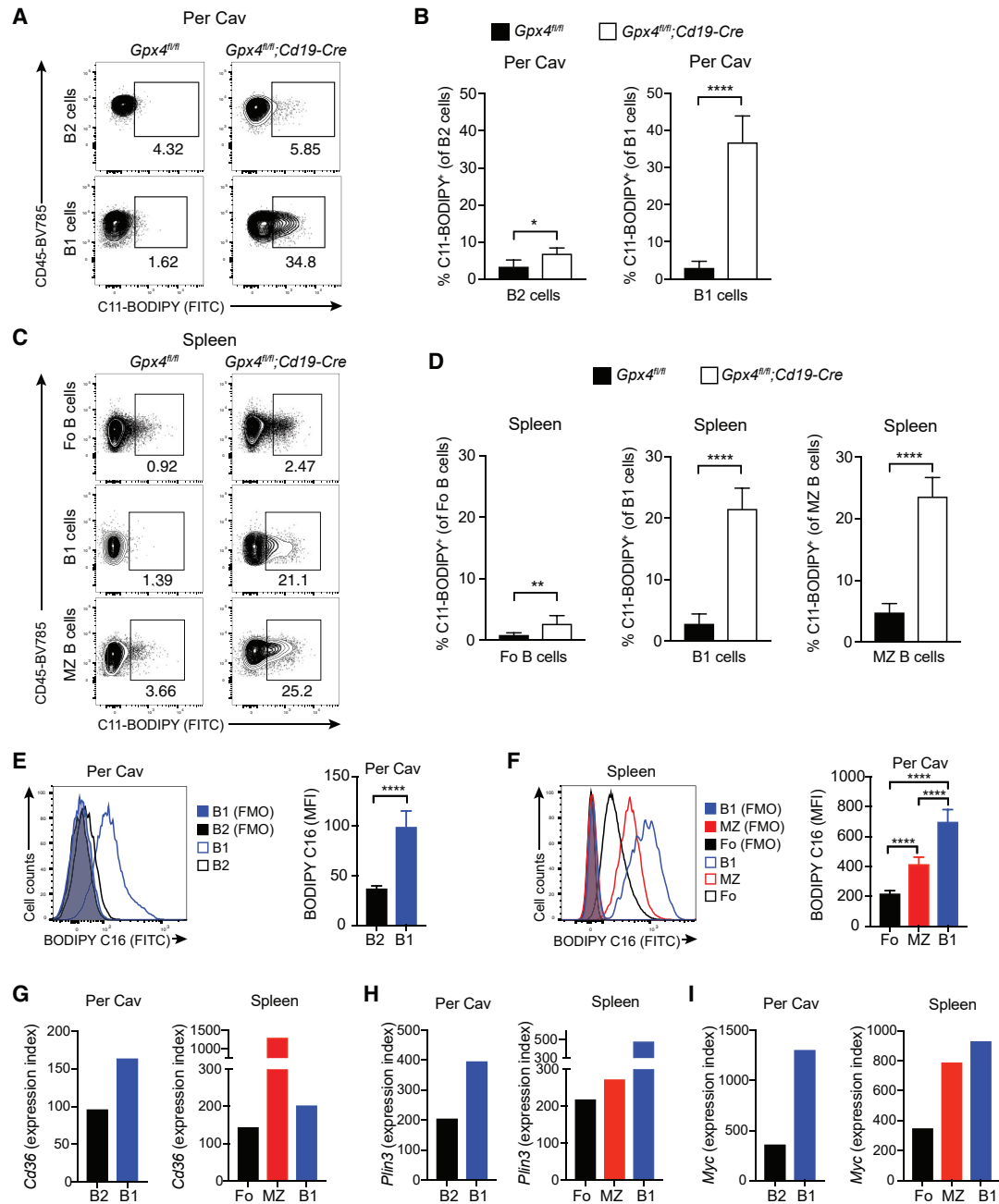


Figure 5. *Gpx4* Prevents Lipid ROS in B1 and MZ B Cells but Not in Fo B2 Cells

(A–D) The accumulation of lipid peroxidation in the indicated *Gpx4*-sufficient and -deficient B cell populations was determined by staining with the C11-BODIPY_{581/591} (n = 5–6). Representative FACS plots (A) and quantification (B) of lipid ROS in B2 (CD19⁺B220⁺CD43⁺CD23⁺) and B1 (CD19⁺B220^{low}CD43⁺CD23⁺) cells from the peritoneal cavity (Per Cav). Representative FACS plots (C) and quantification (D) of lipid peroxidation in Fo B2 (CD19⁺B220⁺CD43⁺CD23⁺), B1 (CD19⁺B220^{low}CD43⁺CD23⁺), and MZ B (CD19⁺B220⁺CD21/35⁺CD23⁺) cells in the spleen.

(E and F) *Gpx4^{fl/fl};Cd19-Cre* and *Gpx4^{fl/fl}* littermate control mice were intravenously injected with BODIPY FL C₁₆ and then analyzed 1 h later. Shown are example distributions of fluorescence (left) and quantification (right) from peritoneal B1 and B2 cells (E) and splenic Fo, MZ B, and B1 cells (F). B1, B2, and MZ B cells were gated as described in (A)–(D) (n = 7).

(G–I) Shown are the mean expression values of *Cd36* (G), *Plin3* (H), and *Myc* (I) in peritoneal B1 and B2 cells (left) and splenic Fo, MZ B, and B1 cells (right). The expression data were obtained from the Immgen database (mean values).

Bar graphs show mean ± SD (B and D–F). Numbers “n” represent individual mice. Numbers in the FACS plots indicate the percentage of the depicted gate. Data are representative of two independent experiments (A–F). Student’s t test (two-tailed, unpaired) was used to compare *Gpx4^{fl/fl};Cd19-Cre* and *Gpx4^{fl/fl}* groups (B, D, and E): *p < 0.05; **p < 0.01; ****p < 0.0001. One-way ANOVA adjusted by Tukey’s multiple comparison test was used in (F): ****p < 0.0002.

See also Figures S4 and S6.

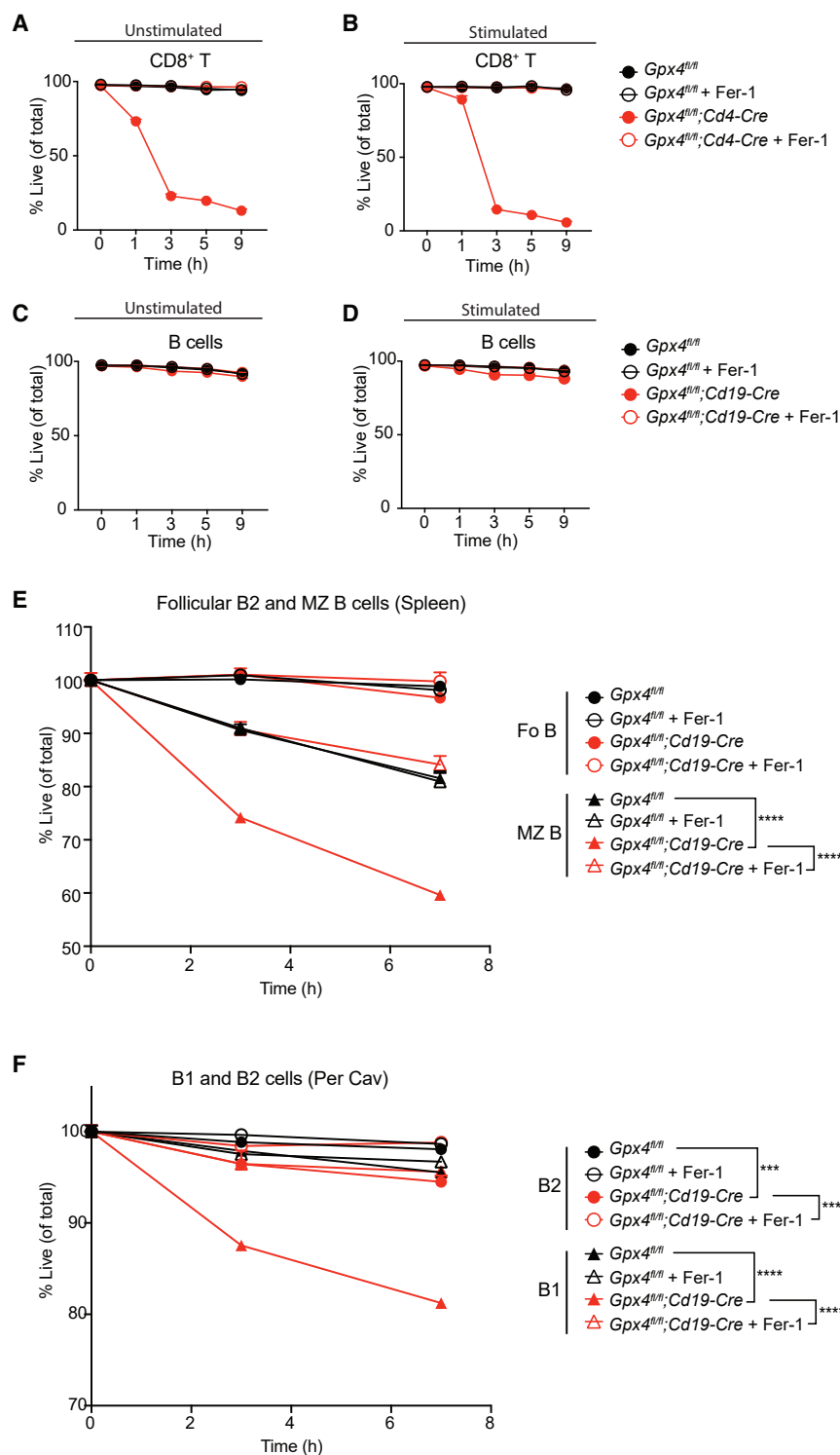


Figure 6. Gpx4-Deficient B1 and MZ B Cells Die by Ferroptosis Ex Vivo

(A–D) Viability of splenic MACS-enriched CD8⁺ T cells from *Gpx4*^{fl/fl}; *Cd4-Cre* and *Gpx4*^{fl/fl} mice (A and B) and of total MACS-enriched B cells from the spleen of *Gpx4*^{fl/fl}; *Cd19-Cre* and *Gpx4*^{fl/fl} littermate control mice (C and D) cultured in the presence or absence of the ferroptosis inhibitor Fer-1 was assessed. CD8⁺ T cells were left unstimulated as a control (A) or stimulated with anti-CD3 and anti-CD28 (B) for the indicated time. Total B cells were left unstimulated as a control (C) or stimulated with LPS and anti-IgM (D) as indicated. Cell viability was assessed via flow cytometry by eFluor780 staining (n = 3).

(E and F) Viability of the indicated B cell populations was assessed over time in stimulated conditions (LPS/anti-IgM) in presence or absence of Fer-1 via flow cytometry by eFluor780 staining. Splenic MZ (CD19⁺B220⁺CD21/35⁺CD23⁺) and Fo (CD19⁺B220⁺CD21/35⁺CD23⁺) B cells (E), and B1 (CD19⁺B220^{low}CD43⁺CD23⁺) and B2 (CD19⁺B220⁺CD43⁺CD23⁺) cells from the peritoneal cavity (F) were FACS sorted from *Gpx4*^{fl/fl}; *Cd19-Cre* and *Gpx4*^{fl/fl} littermate controls (n = 2). Graphs show mean ± SD. Numbers “n” represent biological replicates.

Data are representative of two independent experiments. Two-way ANOVA adjusted by Bonferroni’s multiple comparison test was used in (E) and (F), and the statistical significance (****p ≤ 0.0002; ****p ≤ 0.0001) is shown for the time point of 7 h. See also Figure S6.

opment and GC reactions (Akkaya and Pierce, 2019; Jellusova, 2018). Unlike Fo B2 cells, B1 cells reside in close proximity to potential invading microbes and secrete IgM antibodies before encountering pathogens. Moreover, they undergo increased homeostatic proliferation due to their maintenance by self-renewal rather than by *de novo* development (Baumgarth, 2011, 2016). To ensure this, B1 cells thus display increased metabolic activity (Akkaya and Pierce, 2019; Jellusova, 2018). For instance, a recent report demonstrated that B1a cells display a strikingly higher expression profile of glycolytic genes, high fatty acid synthesis, and uptake of lipids, which are stored in lipid droplets with the potential involvement of *Plin3* (Clarke et al., 2018). Although the metabolic requirements of MZ B cells have not been yet

reprogramming and switching to aerobic glycolysis to produce metabolic intermediates for sustenance of cell growth and proliferation (Brand, 1985; Buck et al., 2015; Wang and Green, 2012). Similar to T cells, naive B cells also drastically increase their metabolic activity to sustain rapid proliferation during devel-

extensively studied, here we additionally found that they also have increased expression of glycolytic genes and the transcription factor Myc, which is known to control metabolic reprogramming in T cells (Wang et al., 2011). These data are consistent with previous reports showing higher expression of the glucose

transporter Glut1 and consumption of glucose by MZ B cells compared to Fo B2 cells (Jayachandran et al., 2018; Jellusova et al., 2017). Moreover, we here demonstrated that MZ B cells take up high levels of fatty acids and display higher expression of *Cd36* and *Plin3* than Fo B2 cells, thus suggesting that MZ B cells might have similar metabolic requirements as B1 cells at the steady state.

Lipolysis is the hydrolytic process by which fatty acids are liberated from lipid droplets. Liberated fatty acids not only are precursors of membrane synthesis but can also be utilized as energy substrates. This requires acyl-CoA synthetases (ACSLs), which have the function to activate and shuttle fatty acids into the mitochondria for energy generation by β -oxidation. The fact that innate-like B cells display higher OXPHOS and fat uptake and storage (Clarke et al., 2018) compared to Fo B2 cells is consistent with an active breakdown of lipid droplets to fuel mitochondrial Krebs cycle to generate ATP. Indeed, the release of free fatty acids by autophagy was shown to be critical in B1 cells to sustain mitochondrial OXPHOS (Clarke et al., 2018). In addition to participate in the breakdown of fat droplets, ACSL-mediated activation of fatty acids is also critically required for lipid-droplet formation (Wilfling et al., 2014). Interestingly, the ACSL family member 4 (ACSL4), which enriches cellular membranes with long polyunsaturated omega-6 fatty acids, was described to be an essential component for ferroptosis execution (Doll et al., 2017). Thus, activation of ACSL4 for lipid-droplet formation and lipolysis may facilitate ferroptosis in *Gpx4*-deficient B1 and MZ B cells. Moreover, since high levels of intracellular free fatty acids are known to cause oxidative stress (Hauck and Bernlohr, 2016), innate-like B cells absolutely require *Gpx4* to prevent the potential lipid-peroxidation events that may occur. Therefore, our results suggest that the described distinct lipid metabolism between Fo B2 cells and B1/MZ B cells dictates the requirement of *Gpx4* to scavenge lipid ROS and inhibit ferroptosis. Interestingly, it has been recently reported that B2 cells can differentiate into functional B1 cells upon acquisition of a B1 cell-typical self-reactive B cell receptor through proliferation (Graf et al., 2019). In this regard, it would be interesting to test whether the conversion of B2 into B1 cells also changes their metabolic features and influences their requirement of *Gpx4*.

Gpx4 has a critical role in T cells to prevent lipid peroxidation and ferroptosis during T cell-mediated immune responses *in vivo*. *Gpx4*-deficient CD8⁺ and CD4⁺ T cells failed to expand and to provide protection to viral and parasite infections (Matsushita et al., 2015). By contrast, here we surprisingly found that Fo B2 cells undergo normal development, homeostatic maintenance, GC reactions, and antibody responses in the absence of *Gpx4*. Interestingly, we have previously described that the other main cellular antioxidant pathway, namely, the thioredoxin-1 (Trx1) system, is also strikingly required in T cells but largely dispensable in Fo B2 cells (Muri et al., 2018, 2019). Importantly, however, the absence of Trx1 does not affect lipid peroxidation in T cells as it is the case for the deletion of *Gpx4*, since our previous study pointed out the exclusive requirement of Trx1 to donate reducing equivalents to ribonucleotide reductase for DNA biosynthesis (Muri et al., 2018). By contrast, Fo B2 cells do not require the Trx1 system due to their capacity to tap the GSH-glutaredoxin-1 (Grx1) pathway to ensure adequate reducing power for the

generation of nucleotides (Muri et al., 2019). Therefore, the requirements of two major antioxidant systems, namely, Trx1 and *Gpx4*, is T but not Fo B cell specific, despite the existence of two distinct underlying mechanisms (nucleotide biosynthesis for Trx1 and inhibition of lipid peroxidation for *Gpx4*). We believe that this stronger antioxidant potential of Fo B2 cells, as suggested by their dispensability of both Trx1 and *Gpx4*, is at least partially required to allow secretion of the enormous amounts of antibodies, which are released by B cells after activation and differentiation to plasma cells. Indeed, the assembly of immunoglobulins involves numerous disulfide reactions in the endoplasmic reticulum, leading to ROS cascades and oxidative stress (Aronov and Tirosh, 2016). Consistent with this, other reports showed that the cellular antioxidant Nrf2 pathway is increased during plasma cell differentiation (Bertolotti et al., 2012, 2010). Expression of NADPH oxidases (NOX) in B cells but not T cells and their importance in B cell responses might also further explain the requirement of a stronger antioxidant power in B rather than T cells (Bertolotti et al., 2012). In addition to the stronger antioxidant potential and compensatory redox pathways of Fo B cells in comparison to T cells, other causes might explain the variable sensitivity to ferroptosis between different cell populations. For instance, certain metabolic features, such as the synthesis and availability of vitamin E, which completely reversed the effect of *Gpx4* deficiency in T cells (Matsushita et al., 2015), could dictate the sensitivity to ferroptosis. Moreover, the different expression of lipid-modifying enzymes (i.e., ACSL4; Dixon et al., 2015; Doll et al., 2017; Kagan et al., 2017) or the diverse phospholipid metabolism between different types of lymphocytes might also be the reason for the observed differences in sensitivity to ferroptosis.

GSH is a cellular antioxidant required to buffer ROS and prevent cellular damage. Deficiency of GSH abolishes the metabolic reprogramming that switches T cell metabolism toward increased glycolysis and glutaminolysis due to compromised activation of the mammalian target of rapamycin-1 (mTOR) and of the transcription factors NFAT and Myc (Mak et al., 2017). In addition to its direct ROS scavenging role, GSH also critically provides reducing equivalents to *Gpx4* in T cells in order to prevent lipid ROS and ferroptosis (Matsushita et al., 2015). However, it is not clear yet whether GSH has also a similar antioxidant role in B cell metabolism. Our previous work showed that the reducing power of GSH fuels the Grx1 pathway in B2 cells to sustain nucleotide biosynthesis during proliferation (Muri et al., 2019). By contrast, B1 and MZ B cells do not utilize the reducing power of GSH to sustain the Grx1 system, since this pathway is not efficiently active and cannot sustain cell proliferation (Muri et al., 2019). In keeping with this, we here show that the reducing equivalents of GSH sustain *Gpx4* function in B1 and MZ B cells. Therefore, GSH is differentially utilized in innate-like B1 and MZ B cells and in Fo B2 cells to sustain their metabolic requirements. In the formers, GSH mainly donates electrons to *Gpx4* to allow increased lipid uptake by preventing ferroptosis, whereas in the latter it sustains the biosynthesis of nucleotides downstream of the pentose phosphate pathway via reduction of Grx1.

Ferroptosis has been recently recognized to play a relevant role in cancer biology. Indeed, in some cases the metabolic

reprogramming of cancer cells has been shown to render them more sensitive to ferroptosis. However, it is not yet clear how oncogenic mutations modulate ferroptosis sensitivity and how they influence the oxidation of polyunsaturated fatty acids, which is the most well-characterized downstream event during ferroptosis execution. Thus, a deep understanding of these processes might ultimately contribute to the establishment of novel anti-cancer treatments (Friedmann Angeli et al., 2019; Seibt et al., 2019). It has been described that several forms of leukemia display a CD5⁺ phenotype and that the early generation of B1 cells contributes to the progression of chronic lymphocytic leukemia in mice, although this remains controversial in humans (Gough et al., 2017; Hayakawa et al., 2016). Therefore, exploiting the here-reported increased sensitivity of B1 cells to ferroptosis by targeting Gpx4 function or by modulating levels of cysteine and GSH might have profound implications for therapy of B cell leukemia.

STAR★METHODS

Detailed methods are provided in the online version of this paper and include the following:

- KEY RESOURCES TABLE
- LEAD CONTACT AND MATERIALS AVAILABILITY
- EXPERIMENTAL MODEL AND SUBJECT DETAILS
 - Mice
- METHOD DETAILS
 - Bone marrow chimeras
 - Tamoxifen administration
 - Virus infection
 - Immunizations
 - BODIPY C₁₆ uptake *in vivo*
 - Cell suspension preparations
 - Flow cytometry
 - Magnetic cell sorting
 - *In vitro* B cell cultures
 - *In vitro* T cell cultures
 - Antibody measurement by ELISA
 - RNA analysis by RT-quantitative PCR
- QUANTIFICATION AND STATISTICAL ANALYSES
- DATA AND CODE AVAILABILITY

SUPPLEMENTAL INFORMATION

Supplemental Information can be found online at <https://doi.org/10.1016/j.celrep.2019.10.070>.

ACKNOWLEDGMENTS

We are grateful for research grants from ETH Zurich (ETH-23-16-2). We thank Marcus Conrad for providing Gpx4^{hi/n} mice and Martin Bachmann for sharing Qβ-virus-like particles. We further thank members of the ETH Flow Cytometry Core Facility for cell sorting. We acknowledge the use of the Immgen database as an informative tool for our study.

AUTHOR CONTRIBUTIONS

Conceptualization, J.M. and M.K.; Methodology, J.M.; Investigation, J.M. and H.T.; Writing – Original Draft, J.M. and M.K.; Writing – Review & Editing, J.M.

and M.K.; Visualization, J.M.; Supervision, M.K.; Funding Acquisition, M.K.; Resources, G.W.B.; Supervision, M.K.

DECLARATION OF INTERESTS

The authors declare no competing interests.

Received: August 7, 2019

Revised: September 30, 2019

Accepted: October 17, 2019

Published: November 26, 2019

REFERENCES

- Akkaya, M., and Pierce, S.K. (2019). From zero to sixty and back to zero again: the metabolic life of B cells. *Curr. Opin. Immunol.* 57, 1–7.
- Allman, D., and Pillai, S. (2008). Peripheral B cell subsets. *Curr. Opin. Immunol.* 20, 149–157.
- Andreadis, A.A., Hazen, S.L., Comhair, S.A., and Erzurum, S.C. (2003). Oxidative and nitrosative events in asthma. *Free Radic. Biol. Med.* 35, 213–225.
- Aronov, M., and Tirosh, B. (2016). Metabolic Control of Plasma Cell Differentiation- What We Know and What We Don't Know. *J. Clin. Immunol.* 36 (Suppl 1), 12–17.
- Bachmann, M.F., and Zinkernagel, R.M. (1997). Neutralizing antiviral B cell responses. *Annu. Rev. Immunol.* 15, 235–270.
- Bachmann, M.F., Hengartner, H., and Zinkernagel, R.M. (1995). T helper cell-independent neutralizing B cell response against vesicular stomatitis virus: role of antigen patterns in B cell induction? *Eur. J. Immunol.* 25, 3445–3451.
- Baumgarth, N. (2011). The double life of a B-1 cell: self-reactivity selects for protective effector functions. *Nat. Rev. Immunol.* 11, 34–46.
- Baumgarth, N. (2016). B-1 Cell Heterogeneity and the Regulation of Natural and Antigen-Induced IgM Production. *Front. Immunol.* 7, 324.
- Bertolotti, M., Yim, S.H., Garcia-Manteiga, J.M., Masciarelli, S., Kim, Y.J., Kang, M.H., Iuchi, Y., Fujii, J., Vené, R., Rubartelli, A., et al. (2010). B- to plasma-cell terminal differentiation entails oxidative stress and profound re-shaping of the antioxidant responses. *Antioxid. Redox Signal.* 13, 1133–1144.
- Bertolotti, M., Sitia, R., and Rubartelli, A. (2012). On the redox control of B lymphocyte differentiation and function. *Antioxid. Redox Signal.* 16, 1139–1149.
- Birben, E., Sahiner, U.M., Sackesen, C., Erzurum, S., and Kalayci, O. (2012). Oxidative stress and antioxidant defense. *World Allergy Organ. J.* 5, 9–19.
- Brand, K. (1985). Glutamine and glucose metabolism during thymocyte proliferation. Pathways of glutamine and glutamate metabolism. *Biochem. J.* 228, 353–361.
- Brigelius-Flohé, R., and Maiorino, M. (2013). Glutathione peroxidases. *Biochim. Biophys. Acta* 1830, 3289–3303.
- Brownlee, M. (2001). Biochemistry and molecular cell biology of diabetic complications. *Nature* 414, 813–820.
- Buck, M.D., O'Sullivan, D., and Pearce, E.L. (2015). T cell metabolism drives immunity. *J. Exp. Med.* 212, 1345–1360.
- Carlson, B.A., Tobe, R., Yefremova, E., Tsuji, P.A., Hoffmann, V.J., Schweizer, U., Gladyshev, V.N., Hatfield, D.L., and Conrad, M. (2016). Glutathione peroxidase 4 and vitamin E cooperatively prevent hepatocellular degeneration. *Redox Biol.* 9, 22–31.
- Cielens, I., Ose, V., Petrovskis, I., Strelnikova, A., Renhofa, R., Kozlovskaya, T., and Pumpens, P. (2000). Mutilation of RNA phage Qbeta virus-like particles: from icosahedrons to rods. *FEBS Lett.* 482, 261–264.
- Clarke, A.J., Riffelmacher, T., Braas, D., Cornall, R.J., and Simon, A.K. (2018). B1a B cells require autophagy for metabolic homeostasis and self-renewal. *J. Exp. Med.* 215, 399–413.
- Comhair, S.A., Ricci, K.S., Arroliga, M., Lara, A.R., Dweik, R.A., Song, W., Hazen, S.L., Blecker, E.R., Busse, W.W., Chung, K.F., et al. (2005). Correlation of

- systemic superoxide dismutase deficiency to airflow obstruction in asthma. *Am. J. Respir. Crit. Care Med.* 172, 306–313.
- D'Autr aux, B., and Toledano, M.B. (2007). ROS as signalling molecules: mechanisms that generate specificity in ROS homeostasis. *Nat. Rev. Mol. Cell Biol.* 8, 813–824.
- Dixon, S.J. (2017). Ferroptosis: bug or feature? *Immunol. Rev.* 277, 150–157.
- Dixon, S.J., Lemberg, K.M., Lamprecht, M.R., Skouta, R., Zaitsev, E.M., Gleason, C.E., Patel, D.N., Bauer, A.J., Cantley, A.M., Yang, W.S., et al. (2012). Ferroptosis: an iron-dependent form of nonapoptotic cell death. *Cell* 149, 1060–1072.
- Dixon, S.J., Winter, G.E., Musavi, L.S., Lee, E.D., Snijder, B., Rebsamen, M., Superti-Furga, G., and Stockwell, B.R. (2015). Human Haploid Cell Genetics Reveals Roles for Lipid Metabolism Genes in Nonapoptotic Cell Death. *ACS Chem. Biol.* 10, 1604–1609.
- Doll, S., Proneth, B., Tyurina, Y.Y., Panzilius, E., Kobayashi, S., Ingold, I., Irmeler, M., Beckers, J., Aichler, M., Walch, A., et al. (2017). ACSL4 dictates ferroptosis sensitivity by shaping cellular lipid composition. *Nat. Chem. Biol.* 13, 91–98.
- D ber, S., Hafner, M., Krey, M., Lienenklaus, S., Roy, B., Hobeika, E., Reth, M., Buch, T., Waisman, A., Kretschmer, K., and Weiss, S. (2009). Induction of B-cell development in adult mice reveals the ability of bone marrow to produce B-1a cells. *Blood* 114, 4960–4967.
- Finkel, T. (2011). Signal transduction by reactive oxygen species. *J. Cell Biol.* 194, 7–15.
- Finkel, T., and Holbrook, N.J. (2000). Oxidants, oxidative stress and the biology of ageing. *Nature* 408, 239–247.
- Friedmann Angeli, J.P., Schneider, M., Proneth, B., Tyurina, Y.Y., Tyurin, V.A., Hammond, V.J., Herbach, N., Aichler, M., Walch, A., Eggenhofer, E., et al. (2014). Inactivation of the ferroptosis regulator Gpx4 triggers acute renal failure in mice. *Nat. Cell Biol.* 16, 1180–1191.
- Friedmann Angeli, J.P., Krysko, D.V., and Conrad, M. (2019). Ferroptosis at the crossroads of cancer-acquired drug resistance and immune evasion. *Nat. Rev. Cancer* 19, 405–414.
- Ghosn, E.E., Yang, Y., Tung, J., Herzenberg, L.A., and Herzenberg, L.A. (2008). CD11b expression distinguishes sequential stages of peritoneal B-1 development. *Proc. Natl. Acad. Sci. USA* 105, 5195–5200.
- Gough, S.M., Goldberg, L., Pineda, M., Walker, R.L., Zhu, Y.J., Bilke, S., Chung, Y.J., Dufraigne, J., Kundu, S., Jacoby, E., et al. (2017). Progenitor B-1 B-cell acute lymphoblastic leukemia is associated with collaborative mutations in 3 critical pathways. *Blood Adv.* 1, 1749–1759.
- Graf, R., Seagal, J., Otipoby, K.L., Lam, K.P., Ayoub, S., Zhang, B., Sander, S., Chu, V.T., and Rajewsky, K. (2019). BCR-dependent lineage plasticity in mature B cells. *Science* 363, 748–753.
- Hambright, W.S., Fonseca, R.S., Chen, L., Na, R., and Ran, Q. (2017). Ablation of ferroptosis regulator glutathione peroxidase 4 in forebrain neurons promotes cognitive impairment and neurodegeneration. *Redox Biol.* 12, 8–17.
- Hameyer, D., Loonstra, A., Eshkind, L., Schmitt, S., Antunes, C., Groen, A., Bindels, E., Jonkers, J., Krimpenfort, P., Meuwissen, R., et al. (2007). Toxicity of ligand-dependent Cre recombinases and generation of a conditional Cre deleter mouse allowing mosaic recombination in peripheral tissues. *Physiol. Genomics* 31, 32–41.
- Hardy, R.R., Carmack, C.E., Shinton, S.A., Kemp, J.D., and Hayakawa, K. (1991). Resolution and characterization of pro-B and pre-pro-B cell stages in normal mouse bone marrow. *J. Exp. Med.* 173, 1213–1225.
- Hauck, A.K., and Bernlohr, D.A. (2016). Oxidative stress and lipotoxicity. *J. Lipid Res.* 57, 1976–1986.
- Hayakawa, K., Formica, A.M., Brill-Dashoff, J., Shinton, S.A., Ichikawa, D., Zhou, Y., Morse, H.C., 3rd, and Hardy, R.R. (2016). Early generated B1 B cells with restricted BCRs become chronic lymphocytic leukemia with continued c-Myc and low Bmf expression. *J. Exp. Med.* 213, 3007–3024.
- Holodick, N.E., Repetny, K., Zhong, X., and Rothstein, T.L. (2009). Adult BM generates CD5+ B1 cells containing abundant N-region additions. *Eur. J. Immunol.* 39, 2383–2394.
- Jayachandran, N., Mejia, E.M., Sheikholeslami, K., Sher, A.A., Hou, S., Hatch, G.M., and Marshall, A.J. (2018). TAPP Adaptors Control B Cell Metabolism by Modulating the Phosphatidylinositol 3-Kinase Signaling Pathway: A Novel Regulatory Circuit Preventing Autoimmunity. *J. Immunol.* 201, 406–416.
- Jellusova, J. (2018). Cross-talk between signal transduction and metabolism in B cells. *Immunol. Lett.* 201, 1–13.
- Jellusova, J., Cato, M.H., Apgar, J.R., Ramezani-Rad, P., Leung, C.R., Chen, C., Richardson, A.D., Conner, E.M., Benshop, R.J., Woodgett, J.R., and Rickert, R.C. (2017). Gsk3 is a metabolic checkpoint regulator in B cells. *Nat. Immunol.* 18, 303–312.
- Jenner, P. (2003). Oxidative stress in Parkinson's disease. *Ann. Neurol.* 53 (Suppl 3), S26–S36, discussion S36–S38.
- Jennings, G.T., and Bachmann, M.F. (2008). The coming of age of virus-like particle vaccines. *Biol. Chem.* 389, 521–536.
- Kagan, V.E., Mao, G., Qu, F., Angeli, J.P., Doll, S., Croix, C.S., Dar, H.H., Liu, B., Tyurin, V.A., Ritov, V.B., et al. (2017). Oxidized arachidonic and adrenic PES navigate cells to ferroptosis. *Nat. Chem. Biol.* 13, 81–90.
- Lee, P.P., Fitzpatrick, D.R., Beard, C., Jessup, H.K., Lehar, S., Makar, K.W., P rez-Melgosa, M., Sweetser, M.T., Schlissel, M.S., Nguyen, S., et al. (2001). A critical role for Dnmt1 and DNA methylation in T cell development, function, and survival. *Immunity* 15, 763–774.
- Lyras, L., Cairns, N.J., Jenner, A., Jenner, P., and Halliwell, B. (1997). An assessment of oxidative damage to proteins, lipids, and DNA in brain from patients with Alzheimer's disease. *J. Neurochem.* 68, 2061–2069.
- Maiorino, M., Conrad, M., and Ursini, F. (2018). GPx4, Lipid Peroxidation, and Cell Death: Discoveries, Rediscoveries, and Open Issues. *Antioxid. Redox Signal.* 29, 61–74.
- Mak, T.W., Grusdat, M., Duncan, G.S., Dostert, C., Nonnenmacher, Y., Cox, M., Binsfeld, C., Hao, Z., Br stle, A., Itsumi, M., et al. (2017). Glutathione Primes T Cell Metabolism for Inflammation. *Immunity* 46, 675–689.
- Martin, F., Oliver, A.M., and Kearney, J.F. (2001). Marginal zone and B1 B cells unite in the early response against T-independent blood-borne particulate antigens. *Immunity* 14, 617–629.
- Matsushita, M., Freigang, S., Schneider, C., Conrad, M., Bornkamm, G.W., and Kopf, M. (2015). T cell lipid peroxidation induces ferroptosis and prevents immunity to infection. *J. Exp. Med.* 212, 555–568.
- Muri, J., Heer, S., Matsushita, M., Pohlmeier, L., Tortola, L., Fuhrer, T., Conrad, M., Zamboni, N., Kisielow, J., and Kopf, M. (2018). The thioredoxin-1 system is essential for fueling DNA synthesis during T-cell metabolic reprogramming and proliferation. *Nat. Commun.* 9, 1851.
- Muri, J., Thut, H., Heer, S., Krueger, C.C., Bornkamm, G.W., Bachmann, M.F., and Kopf, M. (2019). The thioredoxin-1 and glutathione/glutaredoxin-1 systems redundantly fuel murine B-cell development and responses. *Eur. J. Immunol.* 49, 709–723.
- Pillai, S., and Cariappa, A. (2009). The follicular versus marginal zone B lymphocyte cell fate decision. *Nat. Rev. Immunol.* 9, 767–777.
- Ray, P.D., Huang, B.W., and Tsuiji, Y. (2012). Reactive oxygen species (ROS) homeostasis and redox regulation in cellular signaling. *Cell. Signal.* 24, 981–990.
- Rickert, R.C., Roes, J., and Rajewsky, K. (1997). B lymphocyte-specific, Cre-mediated mutagenesis in mice. *Nucleic Acids Res.* 25, 1317–1318.
- Roveri, A., Maiorino, M., Nisii, C., and Ursini, F. (1994). Purification and characterization of phospholipid hydroperoxide glutathione peroxidase from rat testis mitochondrial membranes. *Biochim. Biophys. Acta* 1208, 211–221.
- Sattler, W., Maiorino, M., and Stocker, R. (1994). Reduction of HDL- and LDL-associated cholesteryl ester and phospholipid hydroperoxides by phospholipid hydroperoxide glutathione peroxidase and Ebselen (PZ 51). *Arch. Biochem. Biophys.* 309, 214–221.
- Seibt, T.M., Proneth, B., and Conrad, M. (2019). Role of GPX4 in ferroptosis and its pharmacological implication. *Free Radic. Biol. Med.* 133, 144–152.
- Seiler, A., Schneider, M., F rster, H., Roth, S., Wirth, E.K., Culmsee, C., Plesnila, N., Kremmer, E., R dmark, O., Wurst, W., et al. (2008). Glutathione

peroxidase 4 senses and translates oxidative stress into 12/15-lipoxygenase dependent- and AIF-mediated cell death. *Cell Metab.* 8, 237–248.

Storni, T., Lechner, F., Erdmann, I., Bächli, T., Jegerlehner, A., Dumrese, T., Kündig, T.M., Ruedl, C., and Bachmann, M.F. (2002). Critical role for activation of antigen-presenting cells in priming of cytotoxic T cell responses after vaccination with virus-like particles. *J. Immunol.* 168, 2880–2886.

Tanigaki, K., Han, H., Yamamoto, N., Tashiro, K., Ikegawa, M., Kuroda, K., Suzuki, A., Nakano, T., and Honjo, T. (2002). Notch-RBP-J signaling is involved in cell fate determination of marginal zone B cells. *Nat. Immunol.* 3, 443–450.

Thomas, J.P., Maiorino, M., Ursini, F., and Girotti, A.W. (1990). Protective action of phospholipid hydroperoxide glutathione peroxidase against membrane-damaging lipid peroxidation. In situ reduction of phospholipid and cholesterol hydroperoxides. *J. Biol. Chem.* 265, 454–461.

Toyokuni, S., Okamoto, K., Yodoi, J., and Hiai, H. (1995). Persistent oxidative stress in cancer. *FEBS Lett.* 358, 1–3.

Victoria, G.D., Schwickert, T.A., Fooksman, D.R., Kamphorst, A.O., Meyer-Hermann, M., Dustin, M.L., and Nussenzweig, M.C. (2010). Germinal center dynamics revealed by multiphoton microscopy with a photoactivatable fluorescent reporter. *Cell* 143, 592–605.

Wang, R., and Green, D.R. (2012). Metabolic checkpoints in activated T cells. *Nat. Immunol.* 13, 907–915.

Wang, R., Dillon, C.P., Shi, L.Z., Milasta, S., Carter, R., Finkelstein, D., McCormick, L.L., Fitzgerald, P., Chi, H., Munger, J., and Green, D.R. (2011). The transcription factor Myc controls metabolic reprogramming upon T lymphocyte activation. *Immunity* 35, 871–882.

Wilfling, F., Haas, J.T., Walther, T.C., and Farese, R.V., Jr. (2014). Lipid droplet biogenesis. *Curr. Opin. Cell Biol.* 29, 39–45.

Yant, L.J., Ran, Q., Rao, L., Van Remmen, H., Shibata, T., Belter, J.G., Motta, L., Richardson, A., and Prolla, T.A. (2003). The selenoprotein GPX4 is essential for mouse development and protects from radiation and oxidative damage insults. *Free Radic. Biol. Med.* 34, 496–502.

STAR★METHODS

KEY RESOURCES TABLE

REAGENT or RESOURCE	SOURCE	IDENTIFIER
Antibodies		
Anti-mouse B220, APC-Cy7, clone RA3-6B2	Biolegend	Cat#103224; RRID: AB_313007
Anti-mouse B220, PerCP, clone RA3-6B2	Biolegend	Cat#103234; RRID: AB_893353
Anti-mouse CD19, APC-Cy7, clone 6D5	Biolegend	Cat#115530; RRID: AB_830707
Anti-mouse CD19, BV650, clone 6D5	Biolegend	Cat#115541; RRID: AB_11204087
Anti-mouse CD21/35, PE, clone 7E9	Biolegend	Cat#123409; RRID: AB_940411
Anti-mouse CD23, Biotin, clone B3B4	Biolegend	Cat#101604; RRID: AB_312829
Anti-mouse CD23, PE, clone B3B4	Thermo Fisher Scientific	Cat#12-0232-83; RRID: AB_465594
Anti-mouse CD24, BV421, clone M1/69	Biolegend	Cat#101825; RRID: AB_10901159
Anti-mouse CD3e, PE, clone 145-2C11	Thermo Fisher Scientific	Cat#12-0031-82; RRID: AB_465496
Anti-mouse CD4, APC, clone GK1.5	BD Biosciences	Cat#553051; RRID: AB_398528
Anti-mouse CD11b, PE, clone M1/70	Biolegend	Cat#101208; RRID: AB_312791
Anti-mouse CD11b, PerCP-Cy5.5, clone M1/70	Biolegend	Cat#101228; RRID: AB_893232
Anti-mouse CD16/32, clone 2.4G2	This paper	N/A
Anti-mouse CD38, PerCP-Cy5.5, clone 90	Biolegend	Cat#102721; RRID: AB_2563332
Anti-mouse CD43, PE-Cy7, clone S11	Biolegend	Cat#143210; RRID: AB_2564349
Anti-mouse CD45, BV785, clone 30-F11	Biolegend	Cat#103149; RRID: AB_2564590
Anti-mouse CD45.1, PerCP-Cy5.5, clone A20	Biolegend	Cat#110728; RRID: AB_893346
Anti-mouse CD45.1, FITC, clone A20	Biolegend	Cat#110706; RRID: AB_313495
Anti-mouse CD45.2, APC, clone 104	Thermo Fisher Scientific	Cat#17-0454-82; RRID: AB_469400
Anti-mouse CD45.2, BV785, clone 104	Biolegend	Cat#109839; RRID: AB_2562604
Anti-mouse CD5, Biotin, clone 53-7.3	Thermo Fisher Scientific	Cat#13-0051-82; RRID: AB_466339
Anti-mouse CD62L, BV421, clone MEL-14	Biolegend	Cat#104435; RRID: AB_10900082
Anti-mouse CD8, FITC, clone 53-6.7	Thermo Fisher Scientific	Cat#11-0081-82; RRID: AB_464915
Anti-mouse CD8, PerCP-Cy5.5, clone 53-6.7	Biolegend	Cat#100734; RRID: AB_2075238
Anti-mouse CD86, FITC, clone GL-1	BD Biosciences	Cat#553691; RRID: AB_394993
Anti-mouse CD93, APC, clone AA4.1	Biolegend	Cat#136509; RRID: AB_2275879
Anti-mouse CD95 (Fas), APC, clone SA367H8	Biolegend	Cat#152604; RRID: AB_2632899
Anti-mouse CXCR4, PE, clone 2B11/CXCR4	BD Biosciences	Cat#551966; RRID: AB_394305
Anti-mouse F4/80, BV421, clone BM8	Biolegend	Cat#123132; RRID: AB_11203717
Anti-mouse Gr-1, PE, clone RB6-8C5	Biolegend	Cat#108408; RRID: AB_313373
Anti-mouse IgD, PE-Cy7, clone 11-26c.2a	Biolegend	Cat#405720; RRID: AB_2561876
Anti-mouse IgM, FITC, clone II/41	Thermo Fisher Scientific	Cat#11-5790-85; RRID: AB_465246
Anti-mouse Ly-6G, BV421, clone 1A8	Biolegend	Cat#127628; RRID: AB_2562567
Anti-mouse NK1.1, PE, clone PK136	Thermo Fisher Scientific	Cat#12-5941-82; RRID: AB_466050
Anti-mouse TCR β , BV421, clone H57-597	Biolegend	Cat#109229; RRID: AB_10933263
Anti-mouse TCR β , PE-Cy7, clone H57-597	Biolegend	Cat#109222; RRID: AB_893625
Anti-mouse TER-119, PE, clone TER-119	Thermo Fisher Scientific	Cat#12-5921-81; RRID: AB_466041
Anti-mouse IgM, AffiniPure F(ab) ₂ Fragment Goat	Jackson ImmuneResearch	Cat#115-005-020; RRID: AB_2338450
Anti-mouse CD3, clone 145-2C11	This paper	N/A
Anti-mouse CD28, clone 37.51	This paper	N/A
Anti-mouse IgM, human ads-AP	SouthernBiotech	Cat#1020-04; RRID: AB_2794200
Anti-mouse IgG2b, human ads-AP	SouthernBiotech	Cat#1090-04; RRID: AB_2794520

(Continued on next page)

Continued

REAGENT or RESOURCE	SOURCE	IDENTIFIER
Bacterial and Virus Strains		
Influenza virus: A/Puerto Rico/8/34, H1N1	provided by Jovan Pavlovic, University of Zurich	N/A
Q β -Virus-like particles (VLPs)	provided by Martin Bachmann, University of Bern	N/A
Bacteria: <i>Streptococcus pneumoniae</i> (strain D39)	provided by Benjamin Marsland, Monash University	N/A
Chemicals, Peptides, and Recombinant Proteins		
Ferostatin-1	Sigma-Aldrich	Cat#SML0583-5MG
Tamoxifen	Sigma-Aldrich	Cat#T5648-1G
Dnase I	Sigma-Aldrich	Cat#4716728001
Collagenase IV	Worthington	Cat#LS004189
LPS	InvivoGen	Cat#tlrl-3pelps
eFluor® 780	Thermo Fisher Scientific	Cat#65-0865-14
Zombie Aqua	Biolegend	Cat#423102
Streptavidin-BV711	BD Biosciences	Cat#563262
Trizol	Thermo Fisher Scientific	Cat#15596018
pNPP	Sigma-Aldrich	Cat#N2765-5
C11-BODIPY581/591	Thermo Fisher Scientific	Cat#D3861
BODIPY FL C16	Thermo Fisher Scientific	Cat#D3821
PC-BSA	Biosearch Technologies	Cat#PC-1011-10
Critical Commercial Assays		
KAPA SYBR® FAST Bio-Rad iCycler® Kit	Sigma-Aldrich	Cat#KK4608
GoScript Reverse Transcriptase Kit	Promega	Cat#A5003
Experimental Models: Organisms/Strains		
Mouse: Gpx4 ^{fl/fl}	Seiler et al., 2008	N/A
Mouse: Cd19-Cre	Rickert et al., 1997	N/A
Mouse: Cd4-Cre	Lee et al., 2001	N/A
Mouse: Cre-ERT2	Hameyer et., 2007	N/A
Mouse: C57BL/6J	The Jackson Laboratory	Cat#JAX:000664; RRID: IMSR_JAX:000664
Mouse: B6.SJL-Ptprc ^a Pepc ^b /BoyJ	The Jackson Laboratory	Cat#JAX:002014, RRID:IMSR_JAX:002014
Oligonucleotides		
Gpx4-FWD: 5'-CTGTGGAATGGATGAAAG-3'	This paper	N/A
Gpx4-REV: 5'-TCAATGAGAACTTGGTAAAG-3'	This paper	N/A
Tbp-FWD: 5'-TTGACCTAAAGACCATTCACCTTC-3'	This paper	N/A
Tbp-REV: 5'-TTCTCATGATGACTGCAGCAAA-3'	This paper	N/A
Software and Algorithms		
FlowJo Software (version 10.4.2)	Three Star	https://www.flowjo.com/
Prism 8 (version 8.0.0)	GraphPad Software	https://www.graphpad.com/scientific-software/prism/
Adobe Illustrator CS6 (version 16.0.4)	Adobe	https://www.adobe.com/
Excel	Microsoft	https://products.office.com/en/excel

LEAD CONTACT AND MATERIALS AVAILABILITY

This study did not generate new unique reagents. Further information and requests for resources and reagents should be directed to and will be fulfilled by the Lead Contact, Manfred Kopf (Manfred.Kopf@ethz.ch).

EXPERIMENTAL MODEL AND SUBJECT DETAILS

Mice

Mice were maintained at the ETH Phenomics Center (EPIC; Zurich, Switzerland) in individually ventilated cages under specific pathogen free conditions. About 6–10 week-old age- and sex-matched mice (either female or male) were used for the experiments and littermates were utilized as controls. The animals presented a healthy status, and none of the mice used in our experiments had been previously used for other procedures. All animal experiments were approved by the local animal ethics committee (Kantonales Veterinärdepartement Zürich) and were performed according to local guidelines (TschV, Zurich) and the Swiss animal protection law (TschG). *Gpx4^{fl/fl}* mice (Seiler et al., 2008) (originally provided by M. Conrad, Helmholtz Zentrum, Munich, Germany) were backcrossed for more than eight generations to C57BL/6. To obtain *Gpx4^{fl/fl};Cd19-Cre*, *Gpx4^{fl/fl};Cre-ERT2* and *Gpx4^{fl/fl};Cd4-Cre* mice, *Gpx4^{fl/fl}* mice were crossed with *Cd19-Cre* (Rickert et al., 1997), *Cre-ERT2* (Hameyer et al., 2007) and *Cd4-Cre* (Lee et al., 2001) mice, respectively. C57BL/6J (CD45.2) and B6.CD45.1 (B6.SJL-Ptprc^aPepr^b/BoyJ) mice were purchased from The Jackson Laboratory (Bar Harbor, Maine, USA).

METHOD DETAILS

Bone marrow chimeras

WT C57BL/6 (CD45.1⁺ CD45.2⁺) recipients were lethally irradiated (9.5 Gy in a RS 2000 [Rad Source Technologies Inc., Alpharetta, USA]). The following day, mice were reconstituted by intravenous injection of bone marrow cells from hind legs of donor mice, treated with antibiotics (0.024% Borgeal, MSD Animal Health, in the drinking water) for 6 weeks, and used for experiments 9 weeks after reconstitution.

Tamoxifen administration

For deletion of the *Gpx4* gene in *Gpx4^{fl/fl};Cre-ERT2* mice, animals were intraperitoneally injected with 2 mg TAM (Sigma-Aldrich) on two consecutive days and used for experiments at least 7 days later.

Virus infection

Influenza virus strain (A/Puerto Rico/8/34, H1N1) was originally provided by J. Pavlovic, University Zurich. Mice at age of 8 weeks were intratracheally infected with 100 plaque-forming units. Mice were bled on day 7 and on day 10 after infection to determine antibody titer in the blood serum. The body temperature and weight of the mice were monitored daily, and animals were euthanized if they fulfilled severity criteria predefined in the approval of these experiments (ZH135/15) by the local animal ethics committee.

Immunizations

For the analysis of GC reactions and antibody responses, mice were intraperitoneally injected with 10 µg of Qβ virus-like particles (Qβ-VLP) containing *Escherichia coli*-derived RNA. The particles were provided by Martin Bachmann and further information about their preparation can be found elsewhere (Cielens et al., 2000; Storni et al., 2002). Mice were bled to assess IgM and IgG2b antibody titers as indicated in each figure. To investigate the antibody response to *Streptococcus pneumoniae*, mice were intravenously injected with 1×10⁸ colony-forming units of heat-inactivated pneumococci (strain D39) and subsequently bled on day 5 to measure IgM antibody responses to phosphorylcholine by ELISA.

BODIPY C₁₆ uptake *in vivo*

Mice were intravenously injected with 50 µg BODIPY FL C₁₆ (Thermo Fisher Scientific) in 200 µL PBS and sacrificed for analysis after 1h. BODIPY FL C₁₆ fluorescence was then determined in the FITC-channel by flow cytometry.

Cell suspension preparations

Mice were mostly sacrificed by CO₂ asphyxiation. When lungs were harvested for analysis, mice were instead sacrificed by an intraperitoneal overdose of sodium pentobarbital. Organs were removed and processed according to the following procedure. Lungs were digested for 45 min at 37°C in IMDM medium (Life Technologies) containing 2 mg/ml of type IV collagenase (Worthington) and 0.02 mg/ml DNaseI (Sigma-Aldrich). All other organs were directly disrupted and passed through a 70 µm cell strainer (Corning). Bone marrow cells were flushed from femurs and tibia, and then directly passed through the 70 µm cell strainer. ACK buffer (home-made) was used for erythrocyte lysis for all organs.

Flow cytometry

Cells were first stained with the Zombie Aqua Fixable Viability kit (Biolegend) or with eFluor780 (eBioscience) to exclude dead cells. For surface staining, cells were resuspended in FACS buffer (PBS +2% FCS), briefly incubated with anti-CD16/CD32 antibody (2.4G2, homemade) to block Fc gamma receptors, and subsequently stained at 4°C with the relevant fluorescently labeled surface antibodies for 20 min. For the detection of lipid peroxidation, cells were stained with 2 µM of the lipid peroxidation sensor C11-BODIPY_{581/591} (Thermo Fisher Scientific) according to the manufacturer's instructions. The signal of the oxidized C11 (FITC channel, green

emission at 530 ± 30 nm) was then monitored, and the percentage of the FITC⁺ population was calculated. A complete list of all antibodies used in this study can be found in the KEY RESOURCES TABLE. Cells were acquired on LSRFortessa or on FACSCanto II, or sorted on FACSaria III (BD Bioscience). Data were analyzed in FlowJo software (Tree Star). All the gating strategies used for flow cytometry plots are shown in [Figures S5 and S6](#).

Magnetic cell sorting

CD19⁺ B cell and total T cell enrichment was achieved by positive selection using a MACS system with microbeads (MACS, Miltenyi Biotec) conjugated to monoclonal anti-mouse CD19 and anti-mouse CD90.2, respectively, following the manufacturer's instructions. Briefly, 100×10^6 cells/ml were stained with microbeads (1:10 dilution) for 15 min at 4°C. After washing, 100×10^6 cells were resuspended in 500 μ L of buffer, and the cell suspension was applied to LS columns and positively sorted in the magnetic field of a MACS separator.

In vitro B cell cultures

MACS-sorted total splenic B cells (CD19⁺) or FACS-sorted B cell populations from the spleen and peritoneal cavity (10^5 /well) were seeded in IMDM + GlutaMAX, 10% FCS, 100 U/mL penicillin, 100 μ g/mL streptomycin, 50 μ M β -mercaptoethanol (all GIBCO) into 96 well plates and stimulated in the presence of AffiniPure F(ab)₂ Fragment Goat anti-mouse IgM (10 μ g/ml; Jackson ImmuneResearch) and LPS from *Escherichia coli* 0111:B4 (1 μ g/ml; InvivoGen). To test the involvement of ferroptosis in B cell survival, the stimulation of B cells was performed in the presence of ferrostatin-1 (Fer-1; 10 μ M; Sigma-Aldrich) as indicated in the figure legend.

In vitro T cell cultures

MACS-sorted T cells (CD90.2⁺) were seeded in IMDM + GlutaMAX, 10% FCS, 100 U/mL penicillin, 100 μ g/mL streptomycin, 50 μ M β -mercaptoethanol (all GIBCO) into 96 well plates pre-coated with anti-CD3 (4 μ g/ml; 145-2C11; home-made) and anti-CD28 (2 μ g/ml; 37.51; home-made) for stimulation (10^5 /well). To analyze cell death by ferroptosis, T cells were stimulated in the presence of ferrostatin-1 (Fer-1; 10 μ M; Sigma-Aldrich) for the indicated times.

Antibody measurement by ELISA

To assess the IgM response to phosphorylcholine, plates were coated with 25 μ g/ml of phosphorylcholine conjugated to bovine serum albumin (PC-BSA, Biosearch Technologies) in PBS. For determination of the antibody response to Q β -VLP in PBS, plates were coated with 1 μ g/ml Q β -VLP. For measurement of influenza virus-specific antibodies, plates were coated with UV-inactivated influenza virus (PR8) in PBS. ELISAs were performed according to standard protocols using alkaline phosphatase (AP)-conjugated secondary antibodies: goat anti-mouse IgM, goat anti-mouse IgG2b (Southern Biotech). After removal of antibodies and a washing step, the alkaline phosphatase p-nitrophenyl phosphate substrate (pNPP; Sigma-Aldrich) was added into each well. Absorbance was then read at 405 nm.

RNA analysis by RT-quantitative PCR

Total RNA was extracted using TRIzol (Life Technologies), followed by reverse transcription using GoScript Reverse Transcriptase (Promega) according to the manufacturer's instructions. Real-time quantitative PCR (RT-PCR) was performed using Brilliant SYBR Green (Sigma-Aldrich) on an i-Cycler (Bio-Rad Laboratories) according to manufacturer's protocol. Expression was normalized to the housekeeping gene *Tbp* for mRNA expression. The sequences of all used primers are listed in the KEY RESOURCES TABLE.

QUANTIFICATION AND STATISTICAL ANALYSES

Statistical significance was determined by either a Student's t test (two-tailed, unpaired), or one-way ANOVA followed by Tukey's corrections, or two-way ANOVA followed by Bonferroni's corrections using Prism software (GraphPad, version 8.0.0). The Student's t test was used to analyze data from two groups, while ANOVA was used for > 2 comparison groups. The method of statistical evaluation is described in each figure legend. Asterisks in figure legends denote statistical significance (*, $p \leq 0.05$; **, $p \leq 0.01$; ***, $p \leq 0.001$; ****, $p \leq 0.0001$ for Student's t test; *, $p \leq 0.0332$; **, $p \leq 0.0021$; ***, $p \leq 0.0002$; ****, $p \leq 0.0001$ for one-way and two-way ANOVA). The data are represented as mean + standard deviation or as mean + standard error of mean as indicated in each figure legend. The number of biological replicates and mice is also defined in the figure legends. The presented data are representative of at least two independent experiments.

DATA AND CODE AVAILABILITY

This study did not generate any datasets.

Cell Reports, Volume 29

Supplemental Information

**B1 and Marginal Zone B Cells but Not
Follicular B2 Cells Require Gpx4
to Prevent Lipid Peroxidation and Ferroptosis**

Jonathan Muri, Helen Thut, Georg W. Bornkamm, and Manfred Kopf

Figure S1

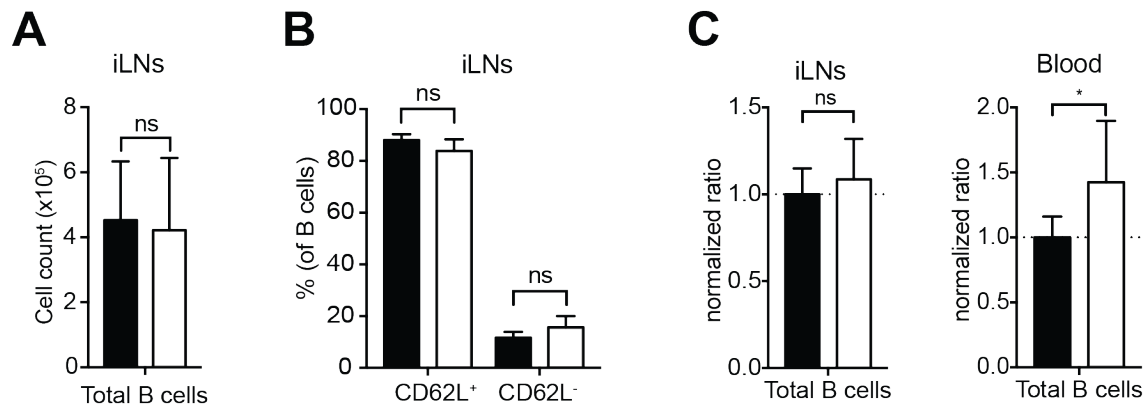


Figure S1. *Gpx4* is dispensable for B-cell homeostasis. Related to Figure 1. (A, B) Analysis of the different B-cell populations in naïve *Gpx4^{fl/fl};Cd19-Cre* and *Gpx4^{fl/fl}* littermate control mice (n = 6). (A) Total cell counts of CD19⁺ B cells in the inguinal lymph nodes (iLNs). (B) Expression of CD62L on CD19⁺ B cells from the iLNs. (C) Lethally irradiated WT mice were reconstituted with a 1:1 mixture of WT and *Gpx4^{fl/fl};Cd19-Cre* bone marrow cells expressing the congenic markers CD45.1 and CD45.2, respectively. After reconstitution, the contribution of *Gpx4^{fl/fl};Cd19-Cre* to the indicated populations in the iLNs (left) and in the blood (right) was assessed. Values were normalized to non-Cre expressing congenic marker-matched TCRβ⁺ T cells, followed by normalization such that CD45.1⁺ WT cell contribution to the respective population equals 1. Values <1 or >1 indicate reduced or higher contribution of *Gpx4^{fl/fl};Cd19-Cre* cells to the B-cell population relative to WT cells, respectively (n = 10). Bar graphs show mean + standard deviation (A-C). Numbers “n” represent individual mice. Data are representative of two independent experiments. Student’s t test (two- tailed, unpaired) was used for the comparison of two groups (A-C): *, P ≤ 0.05; ns, not significant.

Figure S2

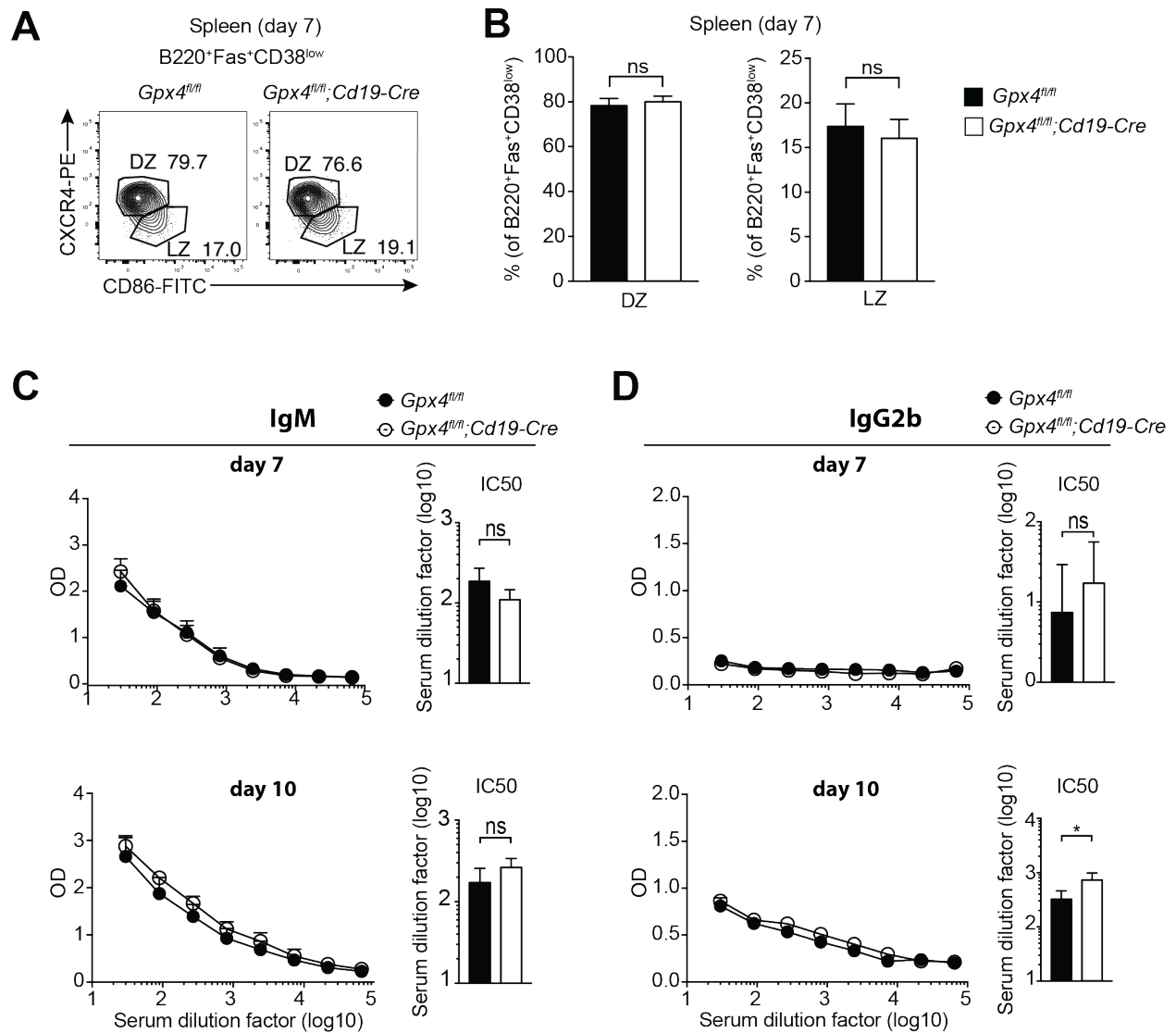


Figure S2. *Gpx4* is not required for B-cell antibody responses and germinal center reactions. Related to Figure 2. (A, B) *Gpx4^{fl/fl};Cd19-Cre* mice and *Gpx4^{fl/fl}* littermate control mice were immunized with Q β -VLPs containing *E. coli* ssRNA. B220⁺Fas⁺CD38^{low} GC B cells were further subdivided into light zone (LZ) and dark zone (DZ) B cells according to expression of CD86 and CXCR4 on day 7 post Q β -VLP immunization. Gating strategy (A) and frequencies (B) of CXCR4⁺CD86⁻ (DZ) and CXCR4⁻CD86⁺ (LZ) B cells are shown (n = 6). (C, D) *Gpx4^{fl/fl};Cd19-Cre* mice and *Gpx4^{fl/fl}* littermate control mice were infected with 100 pfu PR8 influenza A virus. Mice were bled on day 7 (top) and day 10 (bottom) post-infection in order to determine virus-specific IgM (C) and IgG2b (D) antibody responses via ELISA. Each panel depicts plots of OD_{405nm} against serum dilutions (left) and IC50 (right) for virus-specific antibodies (n = 4). Dot plots or bar graphs represent mean + standard deviation (B-D). Numbers “n” represent individual mice. Numbers in the FACS plots indicate the percentage of the depicted gates (A). Data are representative of two independent experiments (A-D). Student's t test (two-tailed, unpaired) was used to compare *Gpx4^{fl/fl};Cd19-Cre* and *Gpx4^{fl/fl}* groups (B-D): *, P \leq 0.05; ns, not significant.

Figure S3

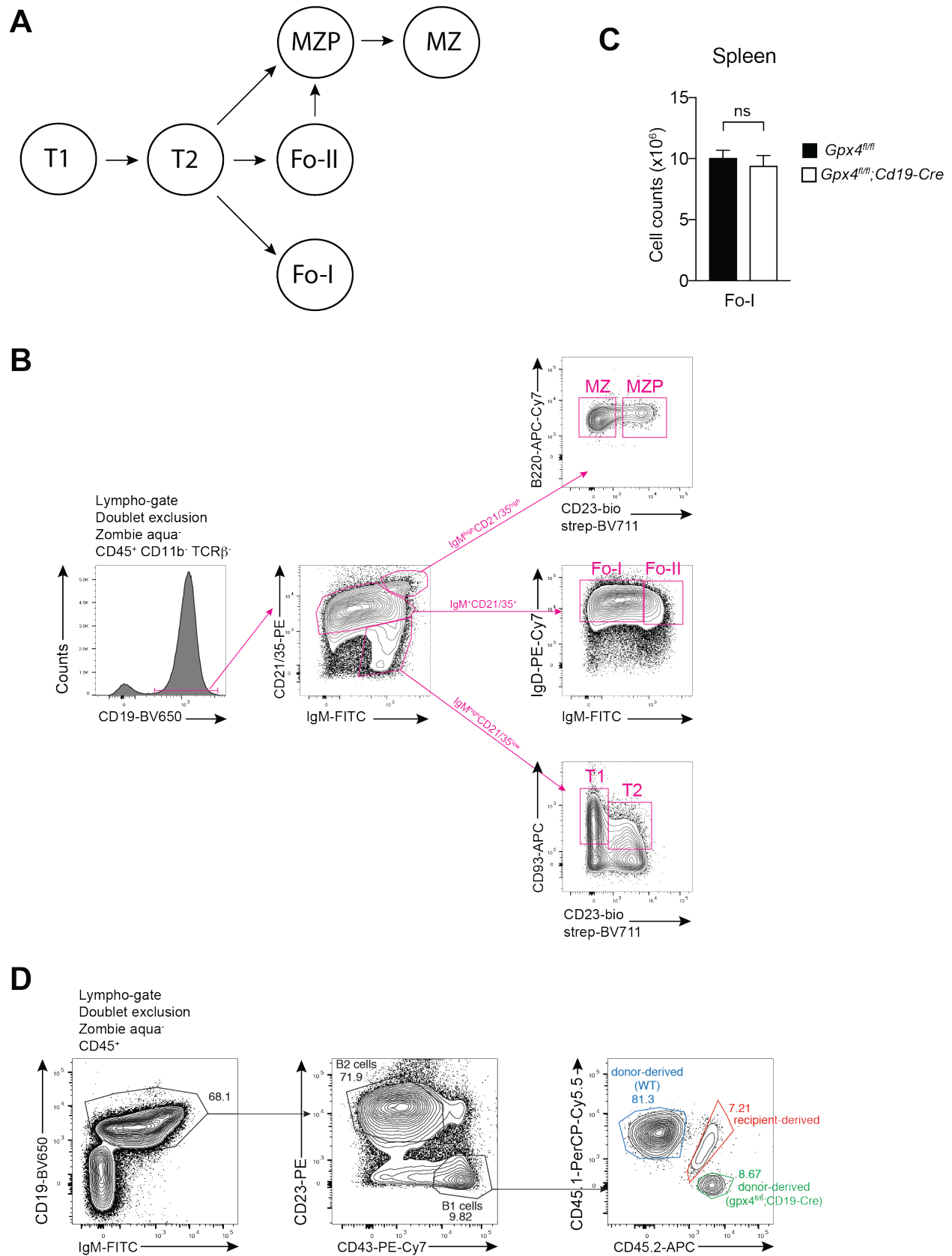


Figure S3. Analysis of the different developing splenic B-cell subsets. Related to Figure 3. (A) Shown is the current model for peripheral B-cell maturation. (B) Gating strategy utilized in this study to identify transitional T1 and T2 cells, follicular (Fo) type I and type II cells, MZ precursors (MZP) and MZ B cells. (C) Total cell counts of Fo type I (Fo-I) in the spleen (n = 6 mice per group). (D) Lethally irradiated WT mice (CD45.1⁺CD45.2⁺) were reconstituted with a 1:1 mixture of WT and *Gpx4^{fl/fl};Cd19-Cre* bone marrow cells expressing the congenic markers CD45.1 and CD45.2, respectively. Shown is the gating strategy utilized to study the potential of Gpx4-sufficient and -deficient bone-marrow to refill the peritoneal B1-cell pool. Bar graphs represent mean + standard deviation (C). Numbers in the FACS plots indicate the percentage of the depicted gates (D). Data are representative of two independent experiments. Student's t test (two-tailed, unpaired) was used to compare *Gpx4^{fl/fl};Cd19-Cre* and *Gpx4^{fl/fl}* groups (C): ns, not significant.

Figure S4

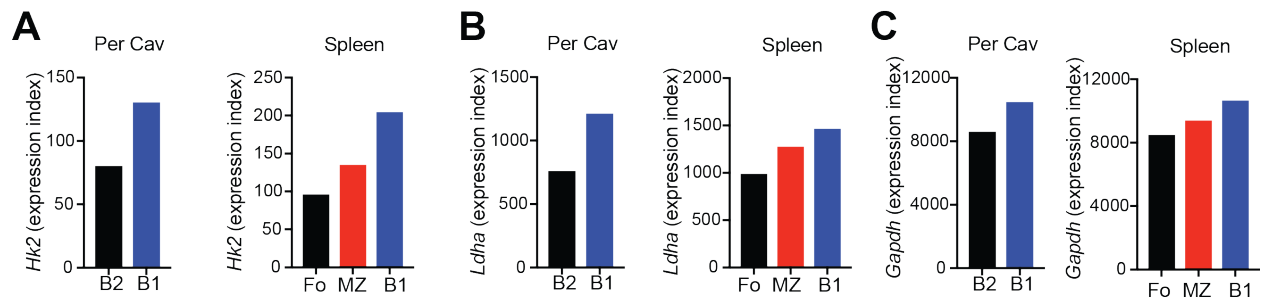


Figure S4. B1 and MZ B cells display increased expression of glycolytic genes. Related to Figure 5. (A-C) Shown are the mean expression values of *Hk2* (A), *Ldha* (B) and *Gapdh* (C) in peritoneal B1 and B2 cells (left) and splenic follicular (Fo), MZ B and B1 cells (right). The expression data were obtained from the Immgen database (mean values).

Figure S5

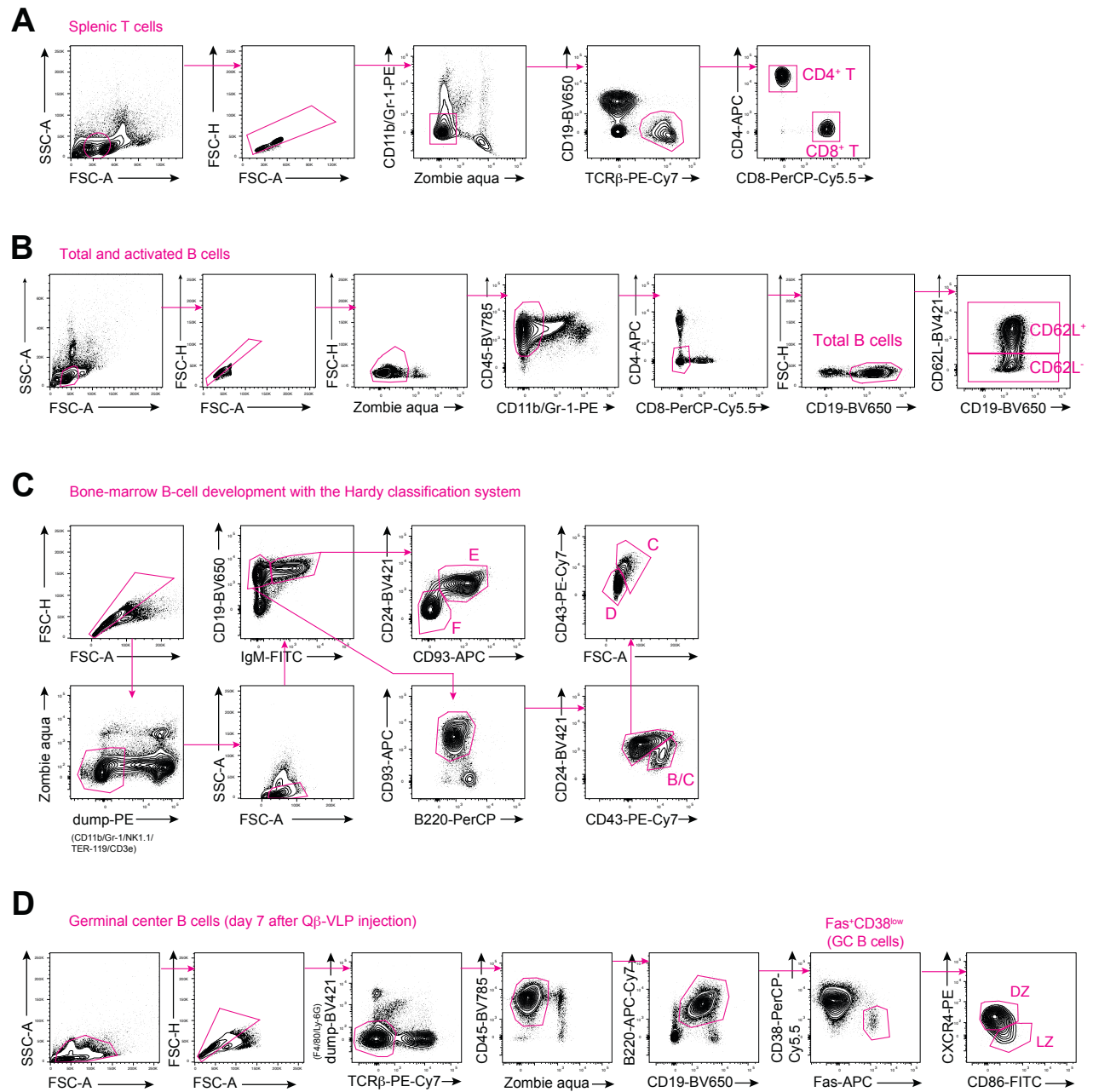
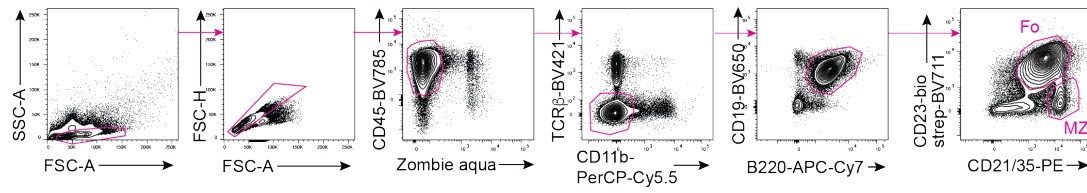


Figure S5. Gating strategies for Figures 1-2. Related to Figures 1-2. (A-C) Representative FACS plots showing gating strategies for Figure 1. **(D)** Representative FACS plots showing the gating strategy for germinal center B cells in Figure 2.

Figure S6

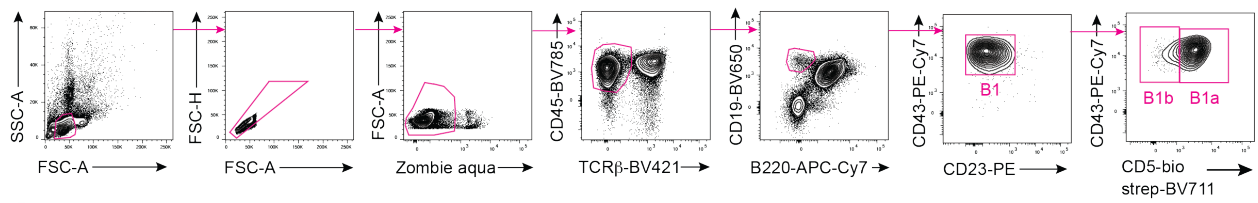
A

Splenic Follicular and MZ B cells



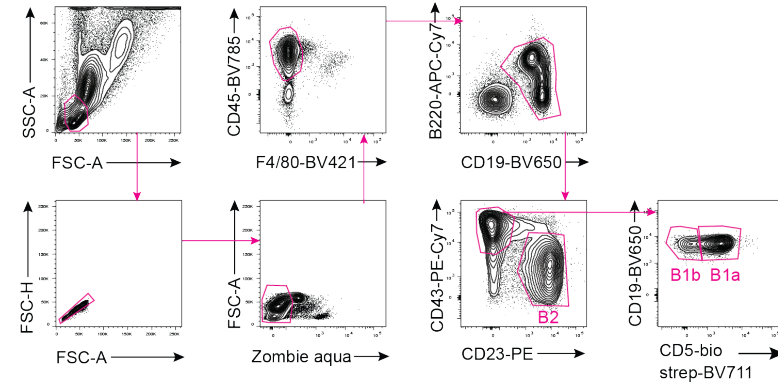
B

Splenic B1 cells



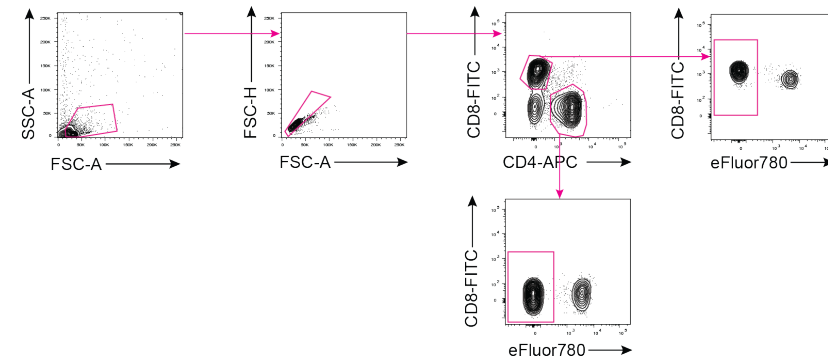
C

B1 and B2 cells in the peritoneal cavity



D

Survival of T cells in vitro



E

Survival of the different B cell populations in vitro

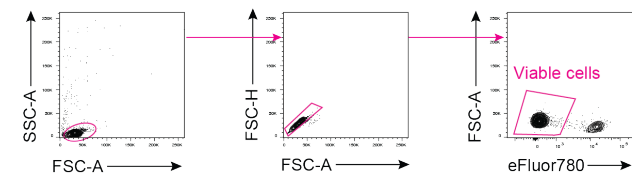


Figure S6. Gating strategies for Figures 3, 5 and 6. Related to Figures 3, 5 and 6.

(A) Representative FACS plots showing gating strategies for follicular B2 and MZ B cells in the spleen (utilized in Figures 3, 5 and 6). (B) Representative FACS plots showing gating strategies for splenic B1 cells (utilized in Figures 3 and 5). (C) Representative FACS plots showing gating strategies for B1 and B2 cells in the peritoneal cavity (utilized in Figures 3, 5 and 6). (D,E) Representative FACS plots showing the gating strategies utilized to study the survival of T cells (D) and of the different B-cell populations (E) in vitro (utilized in Figure 6).